

DOI:10.1002/ejic.201201080

# Copper(II) Complexes with Schiff Bases Containing a Disiloxane Unit: Synthesis, Structure, Bonding Features and Catalytic Activity for Aerobic Oxidation of Benzyl Alcohol

Alina Soroceanu,<sup>[a]</sup> Maria Cazacu,<sup>[a]</sup> Sergiu Shova,<sup>\*,[a]</sup>  
Constantin Turta,<sup>[a]</sup> Jozef Kožíšek,<sup>[b]</sup> Marian Gall,<sup>[b]</sup>  
Martin Breza,<sup>[b]</sup> Peter Rapta,<sup>[b]</sup> Tatiana C. O. Mac Leod,<sup>[c]</sup>  
Armando J. L. Pombeiro,<sup>\*,[c]</sup> Joshua Telser,<sup>[d]</sup> Anatolie A. Dobrov,<sup>[e]</sup>  
and Vladimir B. Arion<sup>\*,[e]</sup>

**Keywords:** Copper(II) complexes / Schiff bases / Chelates / Disiloxane unit / Alcohols / Catalytic oxidation

Mononuclear copper(II) salen-type Schiff base complexes, Cu<sup>II</sup>L<sup>1-5</sup> [H<sub>2</sub>L<sup>1</sup> to H<sub>2</sub>L<sup>5</sup> = tetradentate *N,N,O,O* ligands derived from 2-hydroxybenzaldehyde, 2,4-dihydroxybenzaldehyde, 3,5-dibromo-2-hydroxybenzaldehyde, 2-hydroxy-5-nitrobenzaldehyde, 5-chloro-2-hydroxybenzaldehyde and 1,3-bis(3-aminopropyl)tetramethyldisiloxane, respectively] were prepared in situ in the presence of a copper(II) salt or by direct complexation between a copper(II) salt and a pre-synthesised Schiff base. The compounds {CuL<sup>1</sup>, CuL<sup>1</sup>·0.5Py, CuL<sup>2</sup>·0.375CH<sub>2</sub>Cl<sub>2</sub>, (CuL<sup>3</sup>)[Cu(4-Me-Py)<sub>4</sub>Cl]Cl·2H<sub>2</sub>O, CuL<sup>4</sup>, CuL<sup>4</sup>·CHCl<sub>3</sub> and CuL<sup>5</sup>, as well as the isolated ligand H<sub>2</sub>L<sup>3</sup>} were characterised by elemental analysis, spectroscopic methods (IR, UV/Vis, <sup>1</sup>H NMR, EPR) and X-ray crystallography. The formation of a 12-membered central chelate ring in these complexes is effected by the tetramethyldisiloxane unit, which separates the aliphatic chains, thus significantly reducing the mechanical strain in such a chelate ring. We

dub this a “shoulder yoke effect” by analogy with the load-spreading ability of such an ancient device. The coordination geometry of copper(II) in Cu<sup>II</sup>L<sup>1-5</sup> can be described as tetrahedrally distorted square-planar. Maximum tetrahedral distortion of the coordination geometry expressed by the parameter  $\tau_4$  was observed for CuL<sup>1</sup> (0.460), while distortion was minimal for the two crystallographically independent molecules of CuL<sup>2</sup> (0.219 and 0.284). The Si–O–Si bond angle varies markedly between 169.75(2)° for CuL<sup>1</sup> and 154.2(3)° for CuL<sup>4</sup>·CHCl<sub>3</sub>. Charge-density and DFT calculations on CuL<sup>1</sup> indicate high ionic character of the Si–O bonds in the tetramethyldisiloxane fragment. The new copper(II) complexes bearing the disiloxane moiety have been shown to act as catalyst precursors for the aerobic oxidation of benzyl alcohol to benzaldehyde mediated by the TEMPO radical, reaching yields and TONs up to 99 % and 990, respectively, under mild and environmentally friendly conditions (50 °C; MeCN/H<sub>2</sub>O, 1:1).

## Introduction

Salen-type Schiff bases are among the most versatile ligands known due to their easy preparation and ability to

bind to a variety of metal ions.<sup>[1]</sup> A large number of chiral and achiral salen-type ligands with preferences for different metals have been prepared by straightforward condensation of 2-hydroxybenzaldehyde derivatives with a variety of diamines.<sup>[2]</sup> Their metal complexes can be synthesised either by reaction of metal salts with pre-synthesised Schiff bases in situ or by a condensation reaction of an aldehyde and a (diamine)copper(II) complex.<sup>[3]</sup> This synthetic flexibility has permitted the design of molecular structures with tunable properties (chemical, optical, magnetic, electrical), and numerous derivatives have found applications in many research fields, e.g., biomimetic chemistry,<sup>[4]</sup> analytical chemistry (optical, electrochemical, and chromatographic sensors),<sup>[5]</sup> materials chemistry (light-emitting diodes OLED, PLED)<sup>[6]</sup> and catalysis.<sup>[7]</sup> Schiff base ligands, however, provide only a portion of the binding sites required for octahedral coordination, the remaining sites being available for substrates or small molecules, for example in O<sub>2</sub> activation processes.<sup>[8]</sup> Schiff base metal complexes are of great importance for asymmetric catalysis,<sup>[9]</sup> particularly in the asymmetric epoxidation of unfunctionalised alkenes.<sup>[10–12]</sup> Cop-

[a] “Petru Poni” Institute of Macromolecular Chemistry, Alea Gr. Ghica Voda 41A, 700487 Iasi, Romania  
E-mail: shova@icmpp.ro  
Homepage: <http://www.icmpp.ro>

[b] Department of Physical Chemistry, Slovak University of Technology, Radlinského 9, 81237 Bratislava, Slovak Republic

[c] Centro de Química Estrutural, Instituto Superior Técnico, Technical University of Lisbon, Av. Rovisco Pais, 1049-001 Lisbon, Portugal  
E-mail: pombeiro@ist.utl.pt  
Homepage: [http://cqe.ist.utl.pt/personal\\_pages/pages/armando\\_pombeiro.php](http://cqe.ist.utl.pt/personal_pages/pages/armando_pombeiro.php)

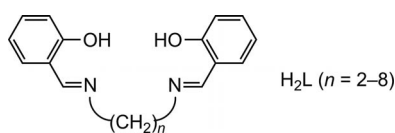
[d] Department of Biological, Chemical and Physical Sciences, Roosevelt University, 430 S Michigan Avenue, Chicago, Illinois 60605, USA

[e] University of Vienna, Institute of Inorganic Chemistry, Währinger Strasse 42, 1090 Vienna, Austria  
E-mail: vladimir.arion@univie.ac.at  
Homepage: <http://anorg-chemie.univie.ac.at/magnoliaPublic/Research/Bioinorganic-chemistry/Researchers/Arion.html>

Supporting information for this article is available on the WWW under <http://dx.doi.org/10.1002/ejic.201201080>.

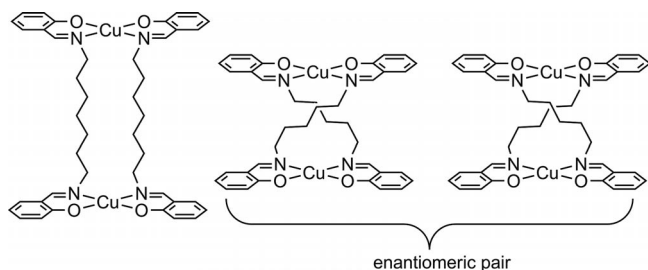
per-salen complexes have proven to be efficient in the selective oxidation of alkanes and alkenes by hydrogen peroxide,<sup>[13]</sup> aromatic hydrocarbons by hydrogen peroxide or *tert*-butyl hydroperoxide,<sup>[14,15]</sup> oxidation of alcohols by hydrogen peroxide,<sup>[16]</sup> stereoselective aldehyde olefination,<sup>[17]</sup> aziridination of olefins,<sup>[18]</sup> conversion of aldehydes into nitro alcohols (asymmetric Henry reaction)<sup>[19]</sup> and asymmetric synthesis of  $\alpha,\alpha$ -disubstituted amino acids.<sup>[20]</sup>

The diamine aliphatic chain length ( $n$ ) determines the type of copper(II) complex formed. Metal-salen-type complexes can be conformationally more rigid or more flexible so as to adopt a variety of geometries such as planar, umbrella-type and stepped conformations.<sup>[7]</sup> Here, 2-hydroxybenzaldehyde reacts with aliphatic diamines to give 2:1 condensation products of the type  $H_2L$  ( $n = 2-8$ ) (Scheme 1).



Scheme 1. Salen-type Schiff bases.

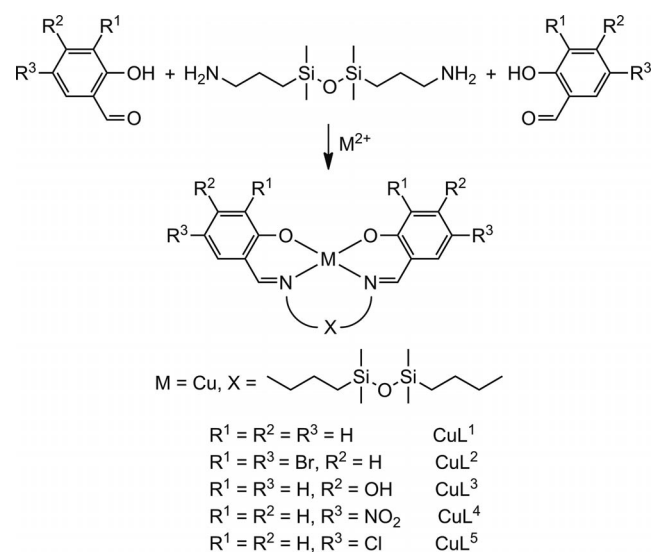
For  $n = 2-4$ , mononuclear metal complexes with chelate ring size alternation 6-5-6,<sup>[21]</sup> 6-6-6<sup>[22]</sup> and 6-7-6<sup>[23]</sup> have been reported. When  $n = 5-8$ , copper(II) complexes with Schiff bases with a 2:2 stoichiometry, as shown in Scheme 2, are well-documented in the literature.<sup>[24,25]</sup> In addition, for  $n = 6$ , pure enantiomers have been isolated, and they crystallise in space groups  $P4_1$  and  $P4_3$  according to an X-ray diffraction study (Scheme 2, right).<sup>[26]</sup> Systems containing intramolecular cavities are themselves of great interest, since they can be used as a reaction field or environment for selective capture, accommodation, transformation or transport of guest molecules.<sup>[25]</sup>



Scheme 2. Cofacial cyclic dimer with 1,7-bis(salicylideneamino)heptane and enantiomerically pure copper(II) complexes with 1,6-bis(salicylideneamino)hexane.

Recently, efforts by us focused on transition-metal complexes using a new ligand type containing a disiloxane group.<sup>[27]</sup> This group possesses unusual structural features,<sup>[28]</sup> namely an Si-O bond length of 1.63 Å, which is small compared with the sum of the Si and O ionic radii and a high and variable bond angle around the O atom, which ranges between 135 and 180° with an energy minimum at 145°.<sup>[29]</sup> In this paper we report on the synthesis and characterisation of mononuclear copper(II) complexes with Schiff bases derived from 2-hydroxybenzaldehyde, 2,4-dihydroxybenzaldehyde, 3,5-dibromo-2-hydroxybenzaldehyde,

2-hydroxy-5-nitrobenzaldehyde or 5-chloro-2-hydroxybenzaldehyde and the disiloxane-bearing diamine 1,3-bis(3-aminopropyl)tetramethyldisiloxane (Scheme 3). The main objectives of the present study consist of (i) the elucidation of the effect of the disiloxane unit on Schiff base formation and its coordinating ability, (ii) insight into the nature of bonding in the disiloxane moiety, which is still disputed in the literature,<sup>[30]</sup> and (iii) evaluation of the catalytic oxidation properties of the new copper(II) complexes. We have a general interest in the metal-catalysed, mild oxidative functionalisation of alkanes and alcohols.<sup>[31-49]</sup> The aerobic oxidation of benzyl alcohol to benzaldehyde mediated by 2,2,6,6-tetramethylpiperidine-1-oxyl (TEMPO) was chosen as a galactose oxidase model reaction to study the catalytic oxidation ability of the copper(II)-salen-type Schiff base complexes bearing a disiloxane moiety.



Scheme 3. Copper(II) complexes prepared in this work.

## Results and Discussion

### Synthesis and Characterisation

The condensation reaction of 2-hydroxybenzaldehyde with 1,3-bis(3-aminopropyl)tetramethyldisiloxane in the presence of three different copper(II) salts (chloride, acetate, nitrate) afforded the metal complex  $CuL^1$ , where  $H_2L^1$  is a tetradentate *N,N,O,O* ligand that contains a tetramethyldisiloxane unit (Scheme 3). The formation of  $CuL^1$  was confirmed by ESI mass spectrometry, which showed peaks at  $m/z = 518, 540$  and  $1057$  attributable to  $[M + H]^+$ ,  $[M + Na]^+$  and  $[2M + Na]^+$ , respectively. The IR spectrum is also in line with the structure proposed for  $CuL^1$  with characteristic stretching vibrations at  $1625\text{ cm}^{-1}$  assigned to the metal-bound azomethine group and absorptions at  $1251, 1081$  and  $799\text{ cm}^{-1}$  typical for a dimethyldisiloxane moiety.<sup>[50]</sup> The complex  $CuL^2$  was prepared by starting from 3,5-dibromo-2-hydroxybenzaldehyde and 1,3-bis(3-aminopropyl)tetramethyldisiloxane in the presence of copper(II) acetate.

The most abundant peak in the positive ESI mass spectrum is at  $m/z = 856$ . The observed isotopic pattern fits well with the theoretical one calculated for  $[M + Na]^+$ . The ligand  $H_2L^3$  was prepared in 77% yield by condensation of 2,4-dihydroxybenzaldehyde with 1,3-bis(3-aminopropyl)tetramethyldisiloxane in a 2:1 molar ratio in methanol at reflux. The formation of the product was verified by FTIR spectroscopy where specific absorption bands are observed at  $1643\text{ cm}^{-1}$  ( $CH=N$ ),  $1253\text{ cm}^{-1}$  ( $Si-CH_3$ ) and  $1045\text{ cm}^{-1}$  ( $Si-O-Si$ ). The  $^1H$  NMR spectrum is also consistent with the suggested structure. Further reaction of  $H_2L^3$  with excess  $CuCl_2 \cdot 2H_2O$  in the presence of 4-methylpyridine afforded the complex  $[CuL^3][Cu(4-Me-Py)_4Cl]Cl \cdot 2H_2O$ . The ESI mass spectrum provided evidence for the formation of  $CuL^3$ . The peaks at  $m/z = 572$  and  $1121$  were assigned to  $[M + Na]^+$  and  $[2M + Na]^+$ . A strong azomethine band at  $1622\text{ cm}^{-1}$  in the FTIR spectrum of the metal complex is shifted by  $21\text{ cm}^{-1}$  relative to that of the free ligand ( $1643\text{ cm}^{-1}$ ), indicating coordination of the azomethine nitrogen atom to the copper(II) ion. Compounds  $CuL^4$  and  $CuL^5$  were prepared in situ by condensation of 2-hydroxy-5-nitrobenzaldehyde and 5-chloro-2-hydroxybenzaldehyde correspondingly with 1,3-bis(3-aminopropyl)tetramethyldisiloxane in a 2:1 molar ratio in the presence of  $CuCl_2 \cdot 2H_2O$  in  $CH_3OH/CH_2Cl_2$  (1:1) and  $CH_3OH/CHCl_3$  (1:1), respectively. Positive-ion ESI mass spectra showed peaks at  $m/z = 608$  and  $630$  for  $CuL^4$  assigned to  $[M + H]^+$  and  $[M + Na]^+$ , respectively, and at  $m/z = 588$  for  $CuL^5$  attributed to  $[M + H]^+$ . The complexes  $CuL^1 \cdot 0.5Py$  and  $CuL^4 \cdot CHCl_3$  were prepared by recrystallisation of  $CuL^1$  and  $CuL^4$  from a solution of pyridine in methanol and chloroform, respectively. The formation of mononuclear copper(II) complexes of  $H_2L^{1-5}$  with a chelate ring size alternation 6–12–6 was confirmed by X-ray diffraction (vide infra). It is also worth noting that metal–salen complexes modified by the Keggin-type polyoxometalate,

namely  $SiW_{11}O_{39}^{8-}$ , apparently consist of the same sequence of chelate rings.<sup>[51]</sup> The formation of even larger 16-membered chelate rings has been found in manganese(II) and nickel(II) complexes with 1,3-bis[3-(imidazol-1-yl)propyl]-1,1,3,3-tetramethyldisiloxane.<sup>[52]</sup>

### X-ray Crystallography

The results of X-ray diffraction studies of  $CuL^1$ ,  $CuL^1 \cdot 0.5Py$ ,  $CuL^2 \cdot 0.375CH_2Cl_2$ ,  $[CuL^3][Cu(4-Me-Py)_4Cl]Cl \cdot 2H_2O$ ,  $CuL^4$ ,  $CuL^4 \cdot CHCl_3$  and  $CuL^5$  are shown in Figures 1, 2, 3, 4, 5, as well as in Figures S1 and S2, respectively.

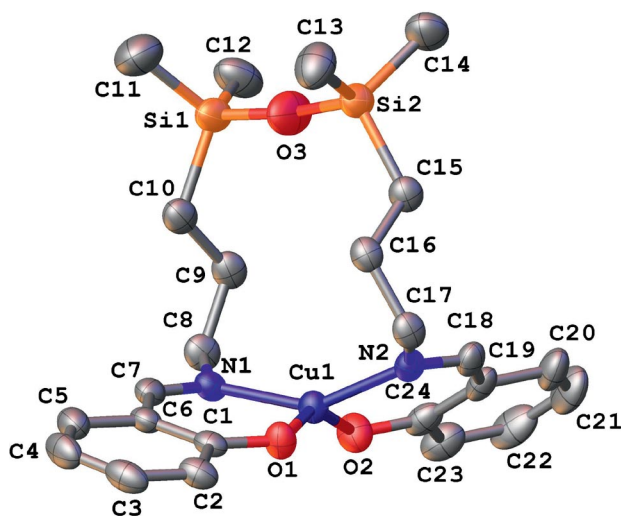


Figure 1. View of the molecule of  $CuL^1$  with atom labelling and thermal ellipsoids at the 50% probability level.

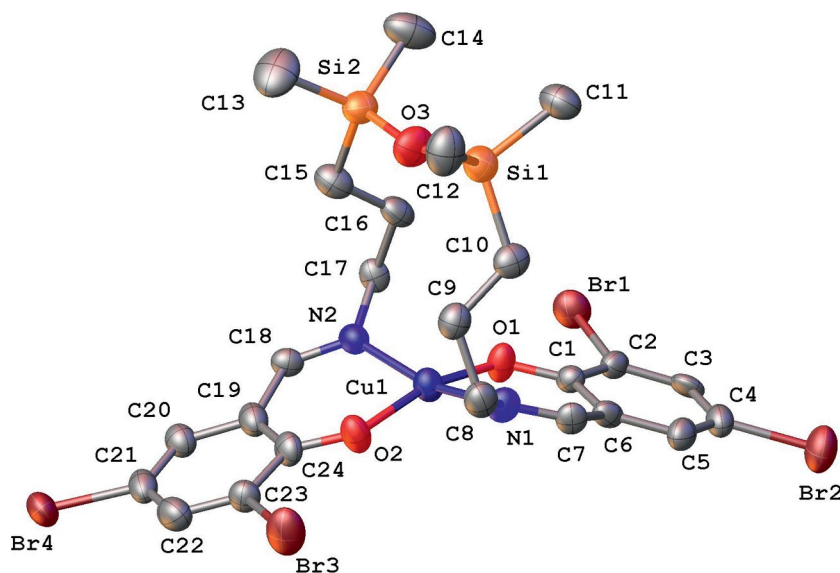


Figure 2. View of the first crystallographically independent molecule (A) of  $CuL^2$  with atom labelling and thermal ellipsoids at the 50% probability level.

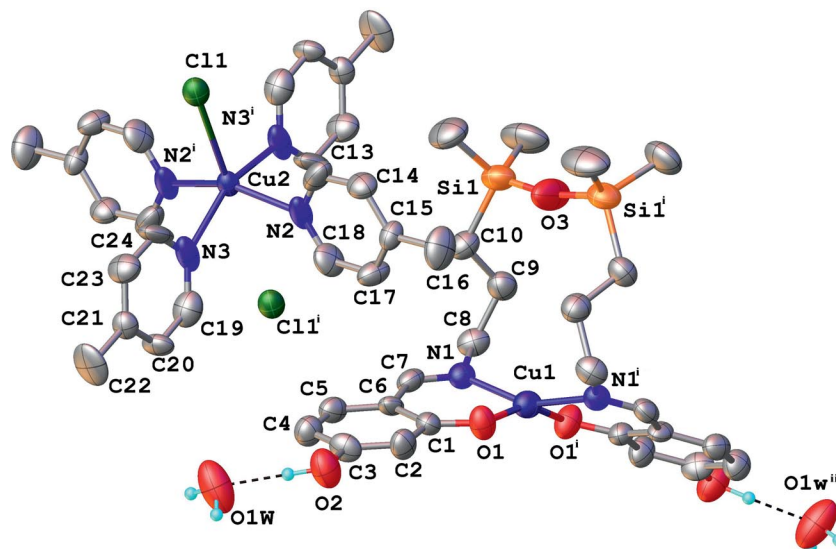


Figure 3. Fragment of the crystal structure of the complex  $[\text{CuL}^3][\text{Cu}(\text{4-Me-Py})_4\text{Cl}]\text{Cl}\cdot 2\text{H}_2\text{O}$  with atom labelling and thermal ellipsoids at the 50% probability level. Only one of two disordered positions for the Cu2 atom is shown. Selected bond lengths [Å] and angles [°]: Cu1–O1 1.912(5), Cu1–N1 1.965(5), Cu2–N2 2.092(6), Cu2–N3 2.118(7), Cu2–C11 2.858(2), Si1–O3 1.604(2); O1–Cu1–O1' 154.4(3), O1–Cu1–N1 92.8(2), O1'–Cu1–N1 92.7(2), N1–Cu1–N1' 155.2(3), N2–Cu2–N3 85.3(2), Si1'–O3–Si1 166.8(5), N2–Cu2–C11 103.8(2), N3–Cu2–C11 102.0(2), Si1'–O3–Si1 166.8(5);  $\tau_4 = 0.357$ ; symmetry code for equivalent atoms: *i*:  $-x + 1, y, -z + 3/2$ ; *ii*:  $1 - x, y, 3/2 - z$ .

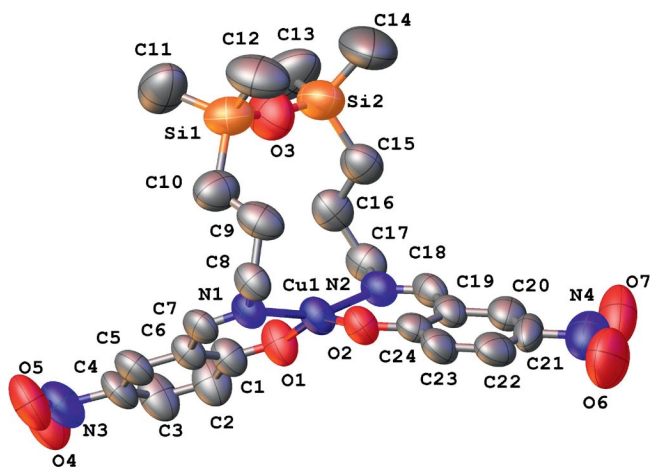


Figure 4. View of the molecule of  $\text{CuL}^4$  with atom labelling and thermal ellipsoids at the 50% probability level.

Compounds  $\text{CuL}^1$ ,  $\text{CuL}^1\cdot 0.5\text{Py}$ ,  $\text{CuL}^2\cdot 0.375\text{CH}_2\text{Cl}_2$ ,  $\text{CuL}^4$ ,  $\text{CuL}^4\cdot \text{CHCl}_3$  and  $\text{CuL}^5$  have a molecular structure in the crystal consisting of the neutral  $[\text{CuL}^n]$  molecules, where  $n = 1, 2, 4$  and 5. On the contrary,  $[\text{CuL}^3][\text{Cu}(\text{4-Me-Py})_4\text{Cl}]\text{Cl}\cdot 2\text{H}_2\text{O}$  has an ionic crystal structure, which is built up from the analogous neutral  $\text{CuL}^3$  complexes,  $[\text{Cu}(\text{4-Me-Py})_4\text{Cl}]^+$  cations,  $\text{Cl}^-$  counter-anions and cocrystallised water molecules in a 1:1:1:2 ratio (Figure 6). The neutral molecule  $\text{CuL}^3$  lies on a twofold crystallographic axis with special positions for the Cu1 and O3 atoms, while Cu2 in the  $[\text{Cu}(\text{4-Me-Py})_4\text{Cl}]^+$  cation is disordered over two resolvable positions around the inversion centre with equal probability (0.5:0.5) (Figure 6). As a result, each Cu2 atom has a square-pyramidal coordination geometry provided by four nitrogen atoms of the 4-Me-Py ligands in the equatorial

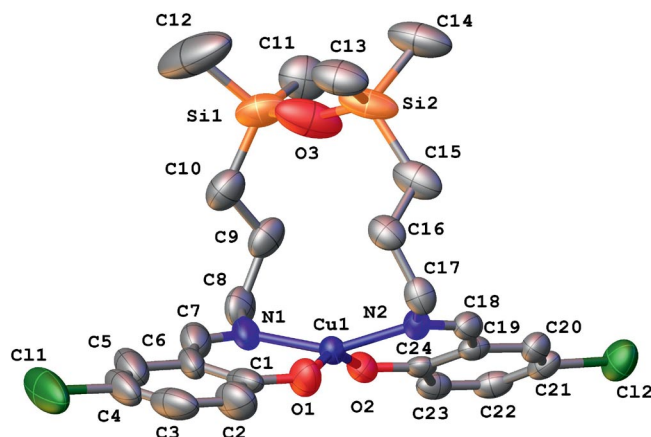


Figure 5. View of the first crystallographically independent molecule (A) of  $\text{CuL}^5$  with atom labelling and thermal ellipsoids at the 50% probability level.

plane and a chlorine atom in the apical position with a Cu2–C11 bond length of 2.858(2) Å. The second Cu2...Cl' contact is equal to 3.812(2) Å. The Cu2 atom comes from the mean plane defined by four nitrogen atoms towards the apical atom C11 by 0.477(1) Å. In  $[\text{CuL}^3]\cdot [\text{Cu}(\text{4-Me-Pic})_4\text{Cl}]\text{Cl}\cdot 2\text{H}_2\text{O}$  there is precedent for noncovalent intermolecular interactions due to the presence of different fragments, which are potential proton donors or proton acceptors. The crystal structure (Figure 6) is characterised as a 3D supramolecular architecture assembled by means of a complex network of O–H...O, O–H...Cl and C–H...Cl hydrogen-bonding interactions.

Compounds  $\text{CuL}^1\cdot 0.5\text{Py}$ ,  $\text{CuL}^2\cdot 0.375\text{CH}_2\text{Cl}_2$  and  $\text{CuL}^5$  crystallise with two independent molecules (denoted as A and B) in the asymmetric unit with close geometrical pa-

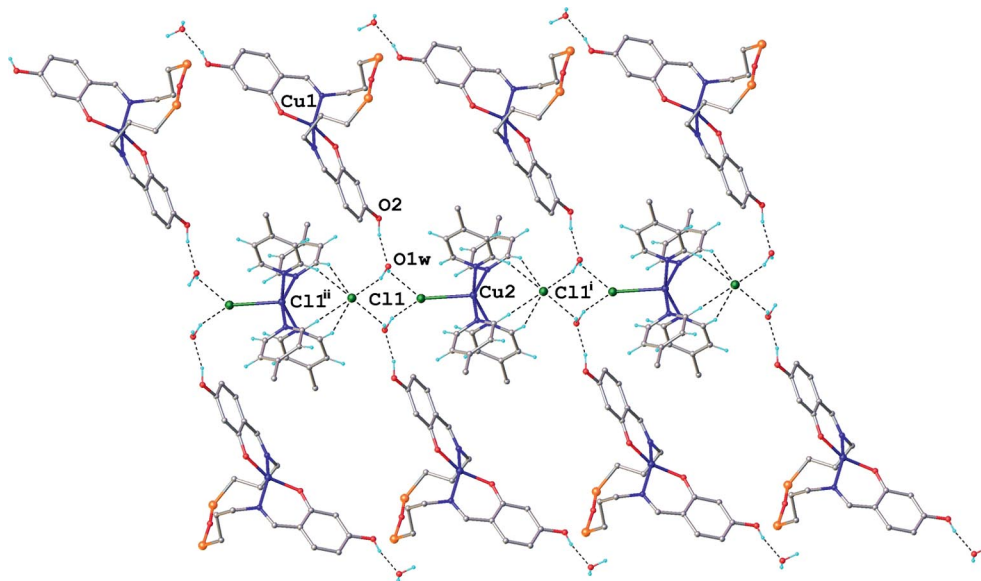


Figure 6. Fragment of the 3D supramolecular network in the crystal structure  $[\text{CuL}^3] \cdot [\text{Cu}(4\text{-Me-Py})_4\text{Cl}] \cdot 2\text{H}_2\text{O}$ . Irrelevant H atoms and siloxane  $\text{CH}_3$  groups are omitted for clarity, hydrogen bonds are shown by dashed lines:  $\text{O2-H} \cdots \text{O1w}$  [ $\text{O2-H}$  0.92,  $\text{H} \cdots \text{O1w}$  1.74,  $\text{O2} \cdots \text{O1w}$  2.628(7) Å;  $\text{O2-H} \cdots \text{O1w}$  160.2°],  $\text{O1w-H} \cdots \text{C11}$  [ $\text{O1w-H}$  0.85,  $\text{H} \cdots \text{C11}$  2.34,  $\text{O1w} \cdots \text{C11}$  ( $1-x, 1-y, 1-z$ ) 3.155(4) Å;  $\text{O1w-H} \cdots \text{C11}$  159.5°],  $\text{C13-H} \cdots \text{C11}$  [ $\text{C13-H}$  0.93,  $\text{H} \cdots \text{C11}$  2.69,  $\text{C13} \cdots \text{C11}$  ( $1-x, -y, 1-z$ ) 3.491(7) Å;  $\text{C13-H} \cdots \text{C11}$  144.2°],  $\text{C24-H} \cdots \text{C11}$  [ $\text{C24-H}$  0.93,  $\text{H} \cdots \text{C11}$  2.62,  $\text{C24} \cdots \text{C11}$  ( $1-x, -y, 1-z$ ) 3.477(7) Å;  $\text{C24-H} \cdots \text{C11}$  152.9°].

rameters. The copper atom in  $\text{CuL}^{1-5}$  is coordinated by a tetradentate  $\text{N}_2\text{O}_2$  Schiff base ligand with the formation of two six- and one twelve-membered chelate rings (Figures 1, 2, 3, 4, and 5, as well as Figures S1 and S2). The coordination geometry of each copper atom can be described as tetrahedrally distorted square-planar. The degree of tetrahedral distortion can be characterised by the parameter  $\tau_4$ , introduced by Houser, to describe the geometry of a four-coordinate metal complex.<sup>[53]</sup> The value of  $\tau_4$  ranges from 1 for perfect tetrahedral geometry to 0 for a perfect square-planar geometry. Intermediate values serve as an indication of tetrahedral distortion of square-planar coordination. The  $\tau_4$  index, calculated for the investigated compounds (Table 1) exhibits values ranging from 0.460 for  $\text{CuL}^1$  to 0.219 for  $\text{CuL}^2 \cdot 0.375 \text{CH}_2\text{Cl}_2$  (0.284 for the other crystallo-

graphically independent molecule in this complex). The Si–O–Si bond angle in the dimethylsiloxane unit falls in the quite broad range between 169.75(2)° for  $\text{CuL}^1$  and 154.2(3)° for  $\text{CuL}^4 \cdot \text{CHCl}_3$ . Even wider variability of this bond is documented in the literature. In quartz it is at 143.7°,<sup>[54]</sup> in hexaphenyldisiloxane this angle is linear,<sup>[55]</sup> while in dioxadisiletane it is 93.5°.<sup>[56]</sup> It should be noted, that the largest Si–O–Si angle in  $\text{CuL}^1$  correlates with the largest distortion of the coordination geometry of copper(II) from square-planar (see  $\tau_4$  value in Table 1). The marked variation of the Si–O–Si angle in the compounds studied indicates the lack of strict directionality of the bonds between the oxygen and silicon atoms, which provides evidence for the predominantly ionic nature of Si–O interactions in the disiloxane moiety. Experimental charge

Table 1. Selected bond lengths [Å] and angles [°] for  $\text{CuL}^1$ ,  $\text{CuL}^1 \cdot 0.5\text{Py}$ ,  $\text{CuL}^2 \cdot 0.375\text{CH}_2\text{Cl}_2$ ,  $\text{CuL}^4$ ,  $\text{CuL}^4 \cdot \text{CHCl}_3$  and  $\text{CuL}^5$ .

	$\text{CuL}^1$	$\text{CuL}^1 \cdot 0.5\text{Py}$		$\text{CuL}^2 \cdot 0.375\text{CH}_2\text{Cl}_2$		$\text{CuL}^4$	$\text{CuL}^4 \cdot \text{CHCl}_3$	$\text{CuL}^5$	
		A	B	A	B			A	B
Cu1–O1	1.882(1)	1.880(3)	1.888(3)	1.884(6)	1.885(6)	1.901(4)	1.893(3)	1.867(4)	1.908(3)
Cu1–O2	1.886(1)	1.886(3)	1.887(3)	1.901(6)	1.902(5)	1.884(3)	1.894(3)	1.900(3)	1.891(3)
Cu1–N1	1.960(2)	1.971(4)	1.972(4)	1.963(7)	1.975(6)	1.974(4)	1.973(3)	1.967(4)	1.970(4)
Cu1–N2	1.963(2)	1.958(4)	1.970(4)	1.975(7)	1.968(6)	1.948(4)	1.984(3)	1.958(4)	1.961(4)
Si2–O3	1.614(2)	1.606(4)	1.616(3)	1.627(7)	1.615(7)	1.639(5)	1.621(4)	1.611(5)	1.611(4)
Si1–O3	1.614(2)	1.610(4)	1.618(4)	1.615(6)	1.624(7)	1.556(5)	1.630(4)	1.606(5)	1.613(4)
O1–Cu1–O2	147.77(7)	151.90(1)	156.56(2)	163.7(3)	160.9(3)	152.76(2)	153.13(1)	151.62(2)	153.41(1)
O1–Cu1–N1	94.52(7)	93.59(2)	92.57(2)	91.5(3)	94.1(3)	93.20(2)	92.95(1)	95.29(2)	93.58(2)
O2–Cu1–N1	95.65(7)	92.48(2)	91.14(2)	90.3(3)	92.7(3)	92.00(2)	92.08(1)	90.40(2)	91.91(2)
O1–Cu1–N2	93.48(6)	92.21(2)	91.36(2)	89.0(3)	88.4(2)	91.84(2)	94.15(1)	93.52(2)	92.04(2)
O2–Cu1–N2	94.26(7)	93.73(2)	93.33(2)	93.3(3)	91.7(2)	93.90(2)	92.88(1)	93.48(2)	93.43(2)
N1–Cu1–N2	147.28(7)	155.07(2)	159.21(2)	165.4(3)	159.0(3)	156.60(2)	153.78(1)	153.77(2)	156.01(1)
Si2–O3–Si1	169.75(2)	165.4(3)	158.4(3)	163.2(5)	161.3(5)	166.4(3)	154.2(3)	158.3(3)	168.3(3)
$\tau_4^{\text{[a]}}$	0.460	0.376	0.314	0.219	0.284	0.359	0.376	0.358	0.387

[a]  $\tau_4 = \frac{360^\circ - (a + \beta)}{141^\circ}$ , where  $a$  and  $\beta$  are the two largest  $\theta$  angles at the Cu atom.

density analysis (vide infra) is a suitable technique to investigate the bonding and electronic characteristics of Si–O bond, something, which is still a matter of debate.<sup>[30,57]</sup>

### EPR Spectroscopy

Each Cu<sup>II</sup> complex with a distinct ligand (i.e., CuL<sup>1</sup>, CuL<sup>2</sup>, CuL<sup>4</sup>, and CuL<sup>5</sup>) was investigated by EPR spectroscopy in 1,2-dichloroethane/*N,N*-dimethylformamide (DCE/DMF, 1:1) frozen solution at 77 K. There was no need to investigate complexes differing only by solvation (i.e., CuL<sup>4</sup>·CHCl<sub>3</sub>), nor the complex with an additional Cu<sup>II</sup> species ([CuL<sup>3</sup>][Cu(4-Me-Py)<sub>4</sub>Cl]Cl·2H<sub>2</sub>O), since this would exhibit overlapping Cu<sup>II</sup> EPR signals. CuL<sup>1</sup>·0.5Py was studied to determine whether the pyridine had an effect in solution. The EPR spectrum for CuL<sup>1</sup> is shown in Figure 7 together with a simulation. The spectrum is of a single species in solution that is of essentially uniaxial symmetry with resolved hyperfine coupling from <sup>63,65</sup>Cu (*I* = 3/2, 100% combined abundance) in the parallel (*g*<sub>||</sub>) region. The values for *g*<sub>||</sub> and *A*<sub>||</sub> of 2.228 and 540 MHz (180 × 10<sup>-4</sup> cm<sup>-1</sup>), respectively, place CuL<sup>1</sup> exactly within the expected region for an overall neutral Cu<sup>II</sup> complex with a d<sub>3/2-y<sup>2</sup></sub> orbital hole and an N<sub>2</sub>O<sub>2</sub> donor set, according to the Peisach and Blumberg correlation.<sup>[58]</sup> Hyperfine coupling from the <sup>14</sup>N ligand atoms is partially resolved in the perpendicular (*g*<sub>⊥</sub>) region, as is often the case,<sup>[59]</sup> but it was not worthwhile to attempt to simulate this effect. In cases of fourfold symmetry about Cu<sup>II</sup>, such as in Cu(OEP) (OEP = 2,3,7,8,12,13,17,18-octaethylporphine dianion), the resolution of ligand <sup>14</sup>N hyperfine coupling is such that it can be well simulated.<sup>[60]</sup> However, any distortions from this ideal geometry can lead to slight ligand inequivalence and/or *g* rhombicity, which makes simulation a challenge. The EPR spectra for the other complexes were very similar to that for CuL<sup>1</sup>, with CuL<sup>5</sup> being nearly identical (see Figure S3),

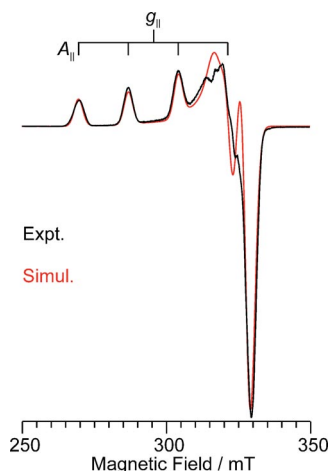


Figure 7. X-band EPR spectrum (black trace) of CuL<sup>1</sup> in DCE/DMF (1:1) frozen solution at 77 K and 9.22 GHz microwave frequency with simulation (red trace). The simulation uses *S* = 1/2, *g* = [2.043, 2.055, 2.228], *A*(<sup>63</sup>Cu) = [50, 50, 540] MHz. Hyperfine coupling to nitrogen ligands is partially resolved in the experimental spectrum, but its simulation was not attempted.

indicating that the chloro substituent has no direct effect on the EPR properties of the Cu<sup>II</sup> site (however, it does affect the catalytic properties – vide infra). Complexes CuL<sup>2</sup> and CuL<sup>4</sup> both showed evidence for a minor (ca. 10%) component in solution, which may be due to (partial) direct DMF coordination and/or to slightly different conformations in solution. Nevertheless, there is overall nothing remarkable about the investigated complexes in the context of EPR spectroscopy of tetragonally distorted Cu<sup>II</sup> systems, except to note that EPR suggests that the complexes are possibly more planar in solution (whether square-planar or square-pyramidal) than would be expected based on their solid-state structures.

### DFT Calculations and Experimental Charge-Density Analysis

Geometry optimisation of CuL<sup>1</sup> led to a perfect *C*<sub>2</sub> molecular symmetry with the *C*<sub>2</sub> rotation axis running through the Cu and O3 atoms. As expected, DFT-optimised bonds are slightly longer than those from X-ray crystallography (Table S1). The above mentioned Houser parameter<sup>[53]</sup>  $\tau_4 = 0.265$  (Table S1) for the DFT-optimised CuL<sup>1</sup> structure (without any solid-state influences) indicates that the tetrahedral distortion is not caused by solid-state effects and should be, to a lower extent, preserved in solution as well. This is in agreement with the largely tetragonal character indicated by the solution EPR spectra and might explain the difficulties in fitting the hyperfine coupling from the <sup>14</sup>N ligand atoms. The calculated Si–O–Si bond angle of 162.5° (Table S1) in the dimethylsiloxane unit, which indicates ionic Si–O bond character (vide infra), is ca. 7° smaller than its experimental value, and this difference may be ascribed to solid-state effects. The geometrical parameters resulting from higher quality X-ray crystallographic data of CuL<sup>1</sup> (Figure S4), which were used for experimental charge-density analysis, can be compared with those obtained from routine X-ray measurement (caption of Figure 1 and Table 1).

As can be seen in Table 2, multipole refinement resulted in a significant improvement of the agreement between the experimental and calculated structure factors. Residual density maps were calculated by a Fourier synthesis where the

Table 2. Summary of the SHELXL and multipole refinement of CuL<sup>1</sup>.

	SHELXL refinement	Multipole refinement
sin $\theta/\lambda$ [Å <sup>-1</sup> ]	1.13	1.13
<i>N</i> <sub>obsd.</sub>	21074	448105
<i>N</i> <sub>v</sub>	289	306
<i>R</i> ( <i>F</i> )	–	0.0194
<i>R</i> ( <i>F</i> ) <sup>[a]</sup>	–	0.0362
<i>wR</i> ( <i>F</i> ) <sup>[a]</sup>	–	0.0133
<i>R</i> ( <i>F</i> <sup>2</sup> )	0.0274	0.0249
<i>R</i> ( <i>F</i> <sup>2</sup> ) <sup>[a]</sup>	0.0488	0.0282
<i>wR</i> ( <i>F</i> <sup>2</sup> ) <sup>[a]</sup>	0.1012	0.0264
<i>S</i>	1.056	1.9725

[a] All reflections.

coefficients are differences between the observed and calculated structure factors corresponding to the converged multipole model. The maximum and minimum of the residual density are  $+0.84 \text{ e}\text{\AA}^{-3}$  at  $0.51 \text{ \AA}$  from Cu and  $-0.87 \text{ e}\text{\AA}^{-3}$  at  $0.04 \text{ \AA}$  from Cu, respectively. The root-mean-square residual density is  $0.072 \text{ e}\text{\AA}^{-3}$ . This residual density is probably due to poor crystal quality.

Nevertheless, the main features of electron density are reliably determined. The central atom is bound by four co-

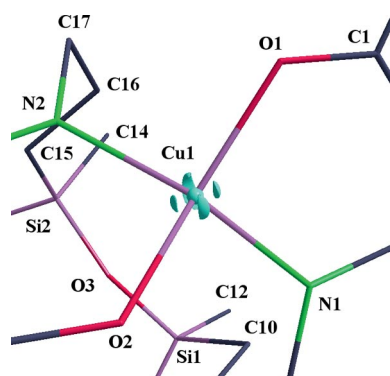


Figure 8. 3D plot of the Laplacian of the electron density around Cu1 at an isosurface value of  $1950 \text{ e}\text{\AA}^{-5}$  for CuL<sup>1</sup>.

ordination bonds to O1, O2, N1 and N2. Inspection of the maximum charge concentrations in the bonding and non-bonding regions in the valence shell, the so-called valence shell charge concentrations (VSCCs) shows that there are four regions of charge concentrations (Figure 8),<sup>[61]</sup> which correspond to non-bonding d-orbitals ( $d_{xz}$ ,  $d_{yz}$ ). On the other hand, the depletion of the charge in the regions where the coordination bonds are formed ( $d_{x^2-y^2}$  orbital) by interaction with the lone pair on oxygen and nitrogen donor atoms (O1, O2, N1 and N2) is clearly seen (Figure 9).

In the framework of the QTAIM<sup>[62]</sup> analysis, the Si–O bonds are highly ionic, as indicated by small electron densities  $\rho$  and their markedly positive Laplacians (Table 3, Figure 10). The second derivative of the electron density, at the bond critical points (BCPs) for two bonds Si1–O3 and Si2–O3 are positive with  $\nabla^2\rho(\mathbf{r}_{\text{BCP}})$  of  $12.05(3)$  and  $14.23(3) \text{ e}\text{\AA}^{-5}$  (Table 3), consistent with that reported for difluorobis[*N*-(dimethylamino)phenylacetimidato-*N,O*]silicon of  $7.373 \text{ e}\text{\AA}^{-5}$  with predominant ionicity for the Si–O bond.<sup>[57]</sup> Our B3LYP calculations produce even higher  $\nabla^2\rho(\mathbf{r}_{\text{BCP}})$  values for the optimised geometry (Table 3). For comparison, B3LYP/6-311G calculations of large NaCl clusters give  $\nabla^2\rho(\mathbf{r}_{\text{BCP}})$  of  $1.41 \text{ e}\text{\AA}^{-5}$  for typically ionic Na–Cl bonds. The ionic Si–O bonding is also confirmed by

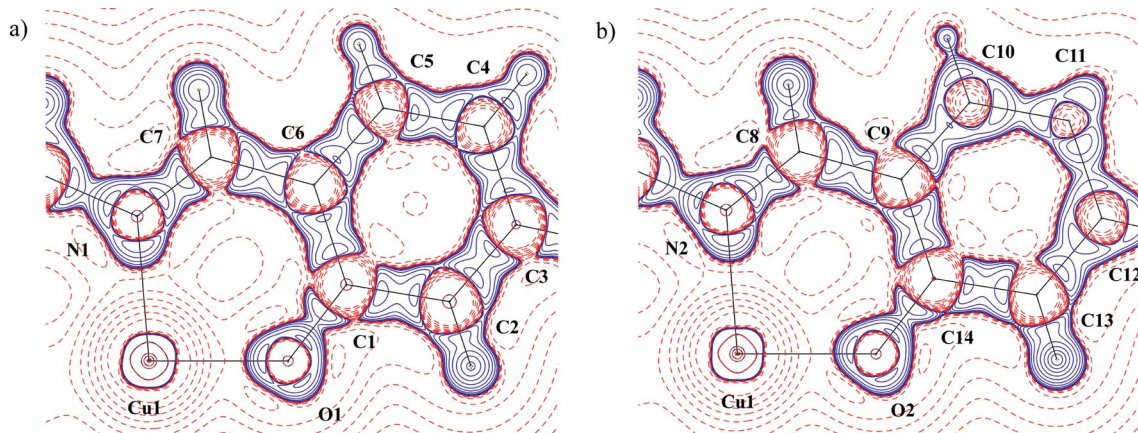


Figure 9. Laplacian distribution  $L(\mathbf{r}) \approx \nabla^2\rho(\mathbf{r})$  in the plane defined by atoms Cu1, O1 and N1 (a) and atoms Cu1, O2 and N2 (b). Contours are drawn at  $-1.0 \times 10^{-3}, \pm 2.0 \times 10^{-2}, \pm 4.0 \times 10^{-1}, \pm 8.0 \times 10^0 \text{ e}\text{\AA}^{-5}$ , with positive contours drawn with a full blue line and negative contours with a broken red line.

Table 3. Selected electron-density properties at bond critical points for CuL<sup>1</sup>.

Bond		Experimental					Theoretical optimised geometry					
Atom A	Atom B	$d_{\text{AB}} [\text{\AA}]$	$\rho_{\text{b}} [\text{e}\text{\AA}^{-3}]$	$\nabla^2\rho_{\text{b}} [\text{e}\text{\AA}^{-5}]$	$\epsilon$	$d_{\text{A}} [\text{\AA}]$	$d_{\text{B}} [\text{\AA}]$	$d_{\text{AB}} [\text{\AA}]$	$\rho_{\text{b}} [\text{e}\text{\AA}^{-3}]$	$\nabla^2\rho_{\text{b}} [\text{e}\text{\AA}^{-5}]$	$\epsilon$	
Cu	O1	1.8898	0.712(2)	15.524(4)	0.07	0.9396	0.9503	1.9240	0.5999	12.3048	0.01	
Cu	O2	1.8993	0.666(2)	15.118(4)	0.08	0.9408	0.9585	1.9241	0.5999	12.3048	0.01	
Cu	N1	1.9693	0.651(2)	11.546(3)	0.03	0.9728	0.9965	1.9877	0.5993	9.5961	0.01	
Cu	N2	1.9703	0.617(1)	11.756(4)	0.03	0.9593	1.0110	1.9877	0.5993	9.5985	0.01	
Si1	O3	1.6325	1.068(7)	12.05(3)	0.01	0.6893	0.9432	1.6578	0.7524	20.1779	0.00	
Si1	C10	1.8783	0.866(5)	-0.76(2)	0.13	0.7629	1.1154	1.8831	0.7187	5.0294	0.07	
Si1	C11	1.8778	0.789(5)	3.21(2)	0.22	0.7456	1.1322	1.8896	0.7234	4.7426	0.07	
Si1	C12	1.8594	1.057(5)	-8.19(2)	0.20	0.8155	1.0439	1.8831	0.7194	5.0077	0.08	
Si2	O3	1.6267	1.087(6)	14.23(3)	0.03	0.6816	0.9451	1.6578	0.7524	20.1779	0.00	
Si2	C13	1.8641	0.842(5)	1.92(2)	0.29	0.7443	1.1197	1.8831	0.7194	5.0294	0.07	
Si2	C14	1.8680	0.946(5)	-3.78(2)	0.18	0.7748	1.0931	1.8831	0.7194	5.0077	0.08	
Si2	C15	1.8687	0.998(5)	-6.67(2)	0.11	0.7934	1.0753	1.8896	0.7234	4.7402	0.07	

NBO population analysis with missing covalent Lewis structures for Si–O bonds. The Lewis structures cannot be found in large NaCl clusters with typically ionic Na–Cl bonds as well. NBO analysis confirmed the highly polarised character of Si–C covalent bonds as indicated by an approximately 28% Si contribution in these bonds (Table S2). Whereas the calculated small positive  $\nabla^2\rho(\mathbf{r}_{\text{BCP}})$  values of Si–C bonds in the optimised  $\text{CuL}^1$  structure indicate non-covalent bonding, some of their experimental counterparts are negative (Table 3). This discrepancy can be ascribed to the errors in experimental data. The values of Si–C BCP ellipticities (Table 3) indicate either small  $\pi$  electron contributions or, more probably, mechanical strain.

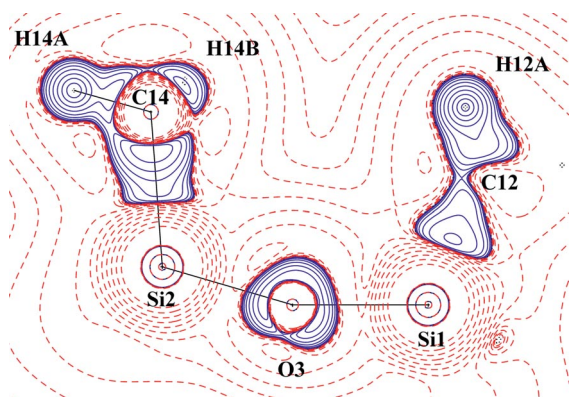


Figure 10. Laplacian distribution  $L(\mathbf{r}) \approx \nabla^2\rho(\mathbf{r})$  in the Si1–O3–Si2 plane. Contours are drawn at  $-1.0 \times 10^{-3}$ ,  $\pm 2.0 \times 10^0$ ,  $\pm 4.0 \times 10^0$ ,  $\pm 8.0 \times 10^0$  ( $n = -3, -2, -1, 0, +1, +2, +3$ )  $\text{e}\text{\AA}^{-5}$ , with positive contours drawn with a full blue line and negative contours with a broken red line.

The VSCCs around O3 revealed an unusual shape (Figure 11).<sup>[61]</sup> The lone pairs of O3 tend to couple from two sides with the silicon bonding vectors, and this is in agreement with the charge in its atomic basin ( $-1.74$  e). On the other hand, the charges in the atomic basins of Si1 and Si2 are of  $+2.71$  and  $+2.76$  e, respectively, in agreement with the predominantly ionic character of the Si–O bonds in the disiloxane unit and consistent with those reported for difluorobis[*N*-(dimethylamino)phenylacetimidato-*N,O*]silicon.<sup>[57]</sup>

In agreement with EPR spectroscopy, the copper oxidation state based on d-electron populations is  $+2$  (see

Tables 4 and 5) with 9 d-electrons (experimental populations seem to be slightly overestimated). Nitrogen charges are less negative than those of either phenolate oxygen (O1, O2) or disiloxane O3 oxygen (O3 being the most negative one). The significantly less positive NBO charges of Si atoms (as well as less negative oxygen and nitrogen charges) might be ascribed to the different type of this population analysis, which is based on wavefunctions. For comparison, B3LYP/6-311G calculations of large NaCl clusters give

Table 4. Population of d orbitals at Cu.

Orbital	Experimental					NBO	
	$d_{x^2-y^2}$	$d_{z^2}$	$d_{yz}$	$d_{xz}$	$d_{xy}$	$\Sigma$	$\Sigma$
[e <sup>-</sup> ]	1.98(1)	1.67(1)	1.82(1)	2.03(1)	2.08(1)	9.58	9.32

Table 5. Charges on selected atoms (e<sup>-</sup>).

Atom	CuI	O1	O2	O3	N1	N2	Si1	Si2
Experimental	–	–	–	–	–	–	2.71	2.76
QTAIM	1.23	1.05	1.03	1.74	0.83	0.90	–	–
NBO	1.33	0.80	0.80	1.25	0.62	0.62	1.89	1.89

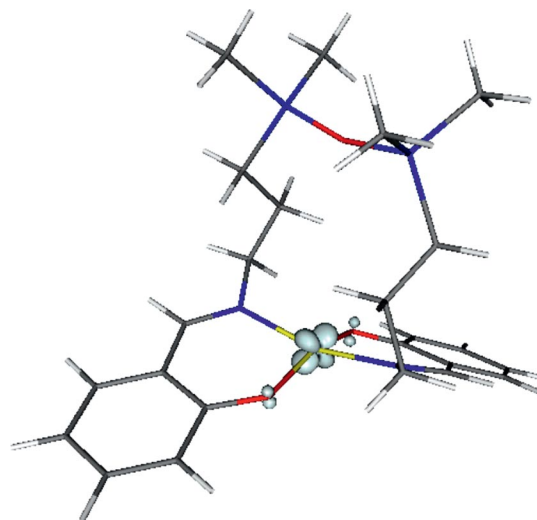


Figure 12. Spin density distribution in  $\text{CuL}^1$  (0.05 a.u. isosurface).

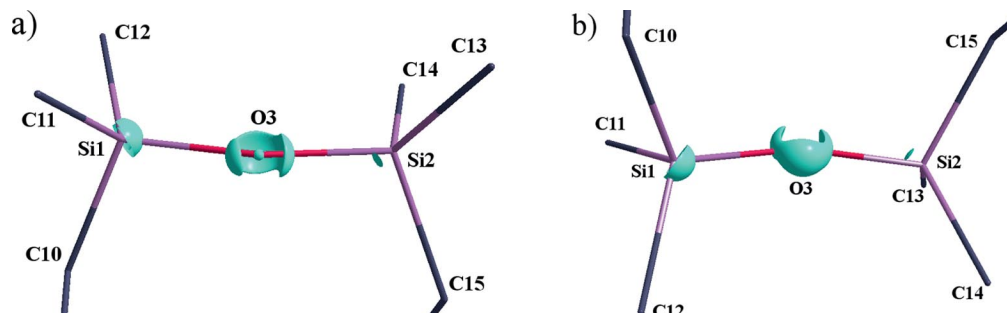


Figure 11. 3D plots of the Laplacian of the electron density around O3 at the isosurface value of  $100 \text{ e}\text{\AA}^{-5}$  from both sides of atom O3 (a) and (b) in  $\text{CuL}^1$ .

NBO charges of  $\pm 0.92$  e, whereas the QTAIM values are  $\pm 0.88$  e. Spin density is mainly located at the  $d_{xz,yz}$  orbitals of copper and  $p_z$  orbitals of oxygen atoms (Figure 12). This distribution cannot be explained by the SOMO (Single Occupied Molecular Orbital) or more exactly the  $\alpha$ -HOMO (Highest Occupied Molecular Orbital) of  $\sigma$ -antibonding Cu–O and Cu–N character, and lower MOs must be employed (see Figure S5, which shows the LUMO through HOMO-8).

One point, which deserves to be addressed here, is the formation of a 12-membered chelate ring upon coordination of a Schiff base containing a disiloxane unit to copper(II). As indicated by preliminary MP2/6-311G\* studies of the energy dependence of  $(\text{CH}_3)_3\text{Si}-\text{O}-\text{Si}(\text{CH}_3)_3$  on the Si–O–Si angle, there is a vanishing rotational energy barrier only for a linear structure (ca.  $0.75 \text{ kcal mol}^{-1}$ ) compared with the optimal  $144^\circ$  bent structure. The high angular flexibility of the ionic disiloxane segment along with Si–O bond lengths of  $1.658 \text{ \AA}$  allows for separation of parallel alkyl chains by up to  $3.3 \text{ \AA}$  in length without significant mechanical strain. Note that the  $\text{N1}\cdots\text{N2}$  separation is  $3.927 \text{ \AA}$ , while  $\text{C8}\cdots\text{C17}$  is  $5.616 \text{ \AA}$ . Such chain separation is much less probable in the case of the C–O–C segment (or even the C–C–C segment) because of significantly shorter C–O bonds of  $1.437 \text{ \AA}$  in  $(\text{CH}_3)_3\text{C}-\text{O}-\text{C}(\text{CH}_3)_3$  [or C–C bonds of  $1.540 \text{ \AA}$  in  $(\text{CH}_3)_3\text{C}-\text{CH}_2-\text{C}(\text{CH}_3)_3$ ] and the covalent character of the bonding in them. A much higher energy barrier corresponds to a linear C–O–C structure (ca.  $25.5 \text{ kcal mol}^{-1}$  with respect to the optimal  $124^\circ$  bent structure). As a result, the optimal C $\cdots$ C separation in the C–O–C unit is only of  $2.54 \text{ \AA}$ , and its elongation by up to  $2.87 \text{ \AA}$  should be connected with high energy demands and enormous mechanical strain. Hence, the tetramethyldisiloxane group displays a kind of *shoulder yoke* effect by separating the alkyl chains and significantly reducing the mechanical

strain in the diamine upon formation of a 12-membered ring.

### Catalytic Activity Studies

The aerobic oxidation of benzyl alcohol to benzaldehyde mediated by TEMPO was chosen as a galactose oxidase model reaction for studying the catalytic oxidation ability of the copper(II) salen-type Schiff base complexes bearing a disiloxane moiety, according to the overall reaction of Equation (1). The obtained results are summarised in Table 6 and show that the studied complexes act as efficient catalysts providing yields of up to 99% (based on the alcohol) and turnover numbers (TONs) up to ca. 990 mol of product per mol of catalyst. Due to the utilisation of TEMPO, which acts as a radical scavenger in preventing the subsequent free radical autoxidation of aldehyde to acid, the system exhibits a remarkably high selectivity towards the formation of benzaldehyde ( $> 99\%$ ), as confirmed by mass balances.<sup>[63]</sup> According to GC–MS analysis, only traces of benzoic acid were identified under the applied reaction conditions, i.e. no significant further oxidation of benzaldehyde to the carboxylic acid was detected. Control reactions carried out either in the absence of the metal com-

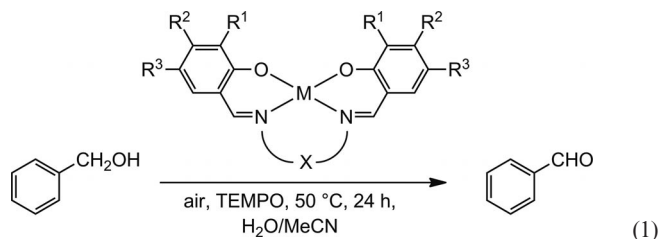


Table 6. Activity of the copper(II) salen-type Schiff base complexes in the aerobic oxidation of benzyl alcohol.<sup>[a]</sup>

Entry	Catalyst	Reaction conditions	Yield [%] <sup>[b]</sup>	TON <sup>[c]</sup>	Ref.
1	CuL <sup>1</sup>	MeCN/H <sub>2</sub> O, 50 °C, 24 h	68.4	684	this work
2	CuL <sup>1</sup> ·0.5Py	MeCN/H <sub>2</sub> O, 50 °C, 24 h	70.6	706	this work
3	CuL <sup>2</sup> ·0.375CH <sub>2</sub> Cl <sub>2</sub>	MeCN/H <sub>2</sub> O, 50 °C, 24 h	83.3	833	this work
4	CuL <sup>4</sup>	MeCN/H <sub>2</sub> O, 50 °C, 24 h	76.9	769	this work
5	CuL <sup>4</sup> ·CHCl <sub>3</sub>	MeCN/H <sub>2</sub> O, 50 °C, 24 h	72.1	721	this work
6	CuL <sup>5</sup>	MeCN/H <sub>2</sub> O, 50 °C, 24 h	85.9	859	this work
7	CuL <sup>5</sup>	MeCN/H <sub>2</sub> O, 50 °C, 48 h	98.8	988	this work
8 <sup>[d]</sup>	Cu(NO <sub>3</sub> ) <sub>2</sub>	MeCN/H <sub>2</sub> O, 50 °C, 48 h	27.5	275	this work
9 <sup>[d]</sup>	CuCl <sub>2</sub>	MeCN/H <sub>2</sub> O, 50 °C, 48 h	30.8	308	this work
10 <sup>[d]</sup>	Cu <sup>II</sup> complexes of (hydroxyaryl)hydrazo- $\beta$ -diketones	H <sub>2</sub> O, 80 °C, 6 h	68	68	[32] <sup>[e]</sup>
11 <sup>[d]</sup>	multicopper(II) triethanolamine	H <sub>2</sub> O, 50 °C, 17 h	47	47	[64]
12 <sup>[d]</sup>	Cu(salen)	toluene, 100 °C, 10 h	99	20	[65]
13 <sup>[d]</sup>	self-assembled dicopper(II) diethanolamine cores	H <sub>2</sub> O, 50 °C, 4–48 h	19–99	19–99	[66]
13 <sup>[d]</sup>	Cu <sup>II</sup> -bis(3,5-di- <i>tert</i> -butylsalicylaldehyde)	toluene, 100 °C, 3 h	6–78	18–234	[67]
14 <sup>[d,e]</sup>	Cu <sup>II</sup> -K coordination polymers	H <sub>2</sub> O, 80 °C, 18 h	28–67	28–67	[68]

[a] Reaction conditions: benzyl alcohol (3.0 mmol), catalyst precursor (3  $\mu\text{mol}$ , 0.1 mol-%), TEMPO (0.15 mmol, 5 mol-%), in 5.0 mL of MeCN/aqueous solution of  $\text{K}_2\text{CO}_3$  (1:1) (0.1 mol L<sup>-1</sup>), 50 °C, air (1.0 atm), 24 h, unless stated otherwise. In all cases, selectivity was  $> 99\%$  as shown by mass balances. [b] mol of product/100 mol of substrate. [c] mol of product/mol of catalyst. [d] For comparative purposes. [e] Self-assembled from copper(II) nitrate, potassium hydroxide and azo derivatives of  $\beta$ -diketones, namely 3-(5-chloro-2-hydroxy-3-sulfophenylhydrazo)pentane-2,4-dione or 3-(2-hydroxy-5-nitro-3-sulfophenylhydrazo)pentane-2,4-dione.

plex or without the TEMPO radical indicate that no appreciable alcohol oxidation reaction occurs (yield < 5%).

With regard to the influence of the ligand substituents at the aromatic ring on the catalytic activity, one observes that the presence of an electron-withdrawing substituent (halo or nitro group) has a substantial promoting effect on the activity (Table 6, Entries 3–6 vs. 1, 2). Oxidation catalysed by the phenyl-unsubstituted complex,  $\text{CuL}^1$ , proceeds with only moderate efficiency (benzaldehyde yield of 68%), while the introduction of the chloro substituent, in  $\text{CuL}^5$ , increases the benzaldehyde yield up to 86% (Table 6, Entry 6) under the same experimental conditions. The presence of bromo substituents, in  $\text{CuL}^2$ , has a comparable catalytic enhancing effect (Table 6, Entry 3), whereas a less pronounced influence is exhibited by the nitro group in  $\text{CuL}^4$  (Entries 4 and 5).

The solvent of crystallisation in the sample has a small but measurable effect. The presence of pyridine (a basic species) in the unsubstituted complex results in a slight yield increase (from 68 to 71%, Entries 1 and 2, respectively) whereas chloroform (an acidic compound) in  $\text{CuL}^4$  leads to a slight decrease (from 77 to 72%, Entries 4 and 5, respectively). Prolonging the reaction time to 48 h leads to the quantitative conversion of benzyl alcohol to benzaldehyde (99% yield) by using the catalyst precursor  $\text{CuL}^5$  (Table 6, Entry 7), while the use of  $\text{Cu}(\text{NO}_3)_2$  or  $\text{CuCl}_2$  as a catalyst led to only ca. 30% yield of benzaldehyde (Table 6, Entries 8 and 9), thus showing the importance of  $\text{Cu}^{\text{II}}$  complexation by the Schiff base ligand, as observed<sup>[64–70]</sup> for other N-donor ligands.

In order to search for optimal conditions, the catalyst amount was varied from 0.03 to 0.3 mol-% (i.e., 1–10  $\mu\text{mol}$ ) for the reactions carried out at 50 °C for 24 h (Figure 13), with other conditions remaining constant. A common trend of increasing yield with catalyst amount was observed up to ca. 3  $\mu\text{mol}$  of catalyst, beyond which no further activity increase occurred (Figure 13a). Hence, that catalyst amount was selected for typical experiments as indicated above (Tables 6 and 7). On the other hand, a decrease of the catalyst amount leads to a TON enhancement for all systems (Figure 13b), reaching TONs up to 1750 for 1  $\mu\text{mol}$  of  $\text{CuL}^4$ , although giving a lower yield (59%).

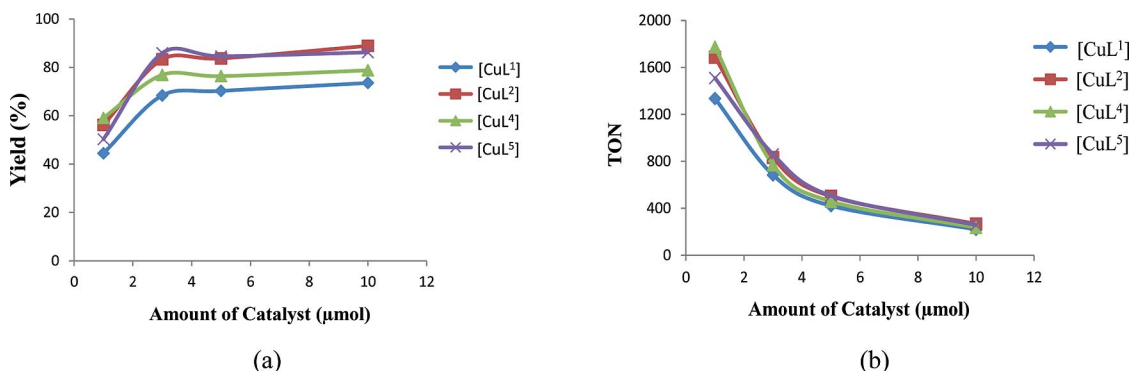


Figure 13. Effect of amount of catalyst on the yield (a) and TON (b) in the aerobic oxidation of benzyl alcohol by copper(II) salen-type Schiff base complexes using TEMPO/air. Reaction conditions: benzyl alcohol (3.0 mmol), catalyst precursor (1–10  $\mu\text{mol}$ ), TEMPO (0.15 mmol, 5 mol-%), in 5.0 mL of MeCN/aqueous  $\text{K}_2\text{CO}_3$  (1:1) solution (0.1 mol L<sup>-1</sup>), 50 °C, air (1.0 atm), 24 h.

Table 7. Activity of the copper(II) salen-type Schiff base complex  $\text{CuL}^5$  in the aerobic oxidation of different alcohols.<sup>[a]</sup>

Entry	Substrate	Yield [%] <sup>[b]</sup>	TON <sup>[c]</sup>
1	benzyl alcohol	85.9	859
2	4-chlorobenzyl alcohol	88.2	882
3	4-methylbenzyl alcohol	76.4	764
4	1-hexanol	11.4	114
5	1-heptanol	6.5	65
6	1-phenylethanol	3.1	31
7	cyclohexanol	2.8	28

[a] Reaction conditions: alcohol (3.0 mmol), catalyst precursor (3  $\mu\text{mol}$ , 0.1 mol-%), TEMPO (0.15 mmol, 5 mol-%), in 5.0 mL of MeCN/aqueous solution of  $\text{K}_2\text{CO}_3$  (1:1) (0.1 mol L<sup>-1</sup>), 50 °C, air (1.0 atm), 24 h. [b] mol of product/100 mol of substrate. [c] mol of product/mol of catalyst.

We have also examined the effects of bases other than  $\text{K}_2\text{CO}_3$  (Figure 14, Table S3) (Supporting Information), but none of the tested ones (NaOH, pyridine or triethylamine) was as effective as carbonate. This is consistent with the

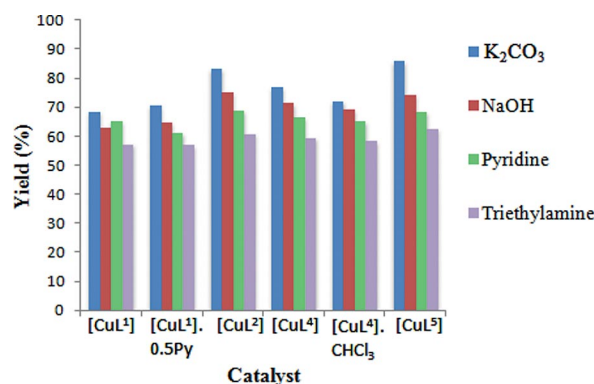


Figure 14. Effect of type of base in the aerobic oxidation of benzyl alcohol by copper(II) salen-type Schiff base complexes using TEMPO/air. Reaction conditions: benzyl alcohol (3.0 mmol), catalyst precursor (3  $\mu\text{mol}$ , 0.1 mol-%), TEMPO (0.15 mmol, 5 mol-%), in 5.0 mL of MeCN/aqueous base (1:1) solution (0.1 mol L<sup>-1</sup>), 50 °C, air (1.0 atm), 24 h.

higher coordinating ability of the other bases, thus competing with the substrate and/or O<sub>2</sub> for coordination to the catalytically active copper centre.

The aerobic oxidation reactions of *para*-substituted (4-chloro- and 4-methyl-)benzyl alcohols were also studied by using the CuL<sup>5</sup>/air/TEMPO system. The former alcohol, bearing an electron-withdrawing substituent, exhibits a higher reactivity than the latter (Table 7, Entries 2 vs. 3), but the relation with the expected<sup>[71]</sup> TEMPO electrophilic attack to the C–H<sub>α</sub> bond is not clear. Conflicting (promoting vs. hampering) effects are found in the literature.<sup>[66,72]</sup> Linear aliphatic alcohols (1-hexanol and 1-heptanol) are much less reactive, leading to yields of only 11 and 6% of the respective aldehydes (Table 7, Entries 4 and 5). Secondary alcohols (1-phenylethanol and cyclohexanol) are not appreciably oxidised to the corresponding ketones (Table 7, Entries 6 and 7). The low catalytic activity concerning secondary alcohols can be attributed to steric hindrance and to the absence of stabilisation by the H-bond of the Cu(O–C'RR')(TEMPOH) intermediate bearing a secondary C radical instead of a primary one,<sup>[71]</sup> and this is in accord with other TEMPO-mediated systems.<sup>[73]</sup>

In summary, the overall yields and TONs (up to 99% and 990, respectively) achieved in this work, under mild conditions, are higher than those observed for other Cu<sup>II</sup> catalysts with triethanolamine,<sup>[64]</sup> diethanolamine,<sup>[66]</sup> salicylaldehyde<sup>[67]</sup> and (hydroxyaryl)hydrazo-β-diketones<sup>[32a,32b]</sup> (Table 6, Entries 10–14). A copper(II)–salen complex<sup>[65]</sup> (Table 6, Entry 12), related to ours, can also bring about efficient alcohol oxidation in terms of yield (99%), but the system requires a higher temperature (100 °C), an unfriendly solvent (toluene), a higher catalyst loading (5 mol-%) and exhibits a lower activity (TON up to 20) in comparison with our catalysts, e.g. CuL<sup>5</sup> (Table 6, Entries 6 and 7), thus showing the importance of the disiloxane moiety in the complexes reported in this work. This can possibly relate to (i) a decrease of the steric hindrance at the metal atom in our complexes having the long disiloxane chain<sup>[70]</sup> (12-membered chelate ring vs. the five-membered ring in the case of the salen ligand), and (ii) the amphiphilic character of the bifunctionalised tetramethyldisiloxane group (coexistence of a hydrophobic moiety with polar coordinated groups), which could promote molecular interactions favourable to the catalytic reaction.<sup>[74]</sup>

Moreover, the high yields of benzaldehyde (relative to the starting benzyl alcohol) obtained with our catalysts are comparable with those achieved when using many other systems. These include self-assembled dicopper(II) diethanolamine cores,<sup>[66]</sup> bis(3,5-di-*tert*-butylsalicylaldehyde)copper(II),<sup>[67]</sup> bis(2-[[4-fluorophenyl]imino]methyl)pyrrolidone)copper(II),<sup>[31b]</sup> Fe<sup>II</sup> and Cu<sup>II</sup> complexes bearing azathia macrocycles,<sup>[69]</sup> CuBr<sub>2</sub>/polymer-based pyridylimine ligand,<sup>[70]</sup> copper coordination polymers based 1-(2,4-difluorophenyl)-1,1-bis[(1*H*-1,2,4-triazol-1-yl)methyl]ethanol<sup>[75]</sup> or other Cu catalytic systems<sup>[68,76]</sup> with bipyridine, pyrazole or Schiff base ligands.

The detailed mechanism of the TEMPO-catalysed oxidation of alcohols (R–CH<sub>2</sub>OH) with the above copper(II)–

salen-type Schiff base complexes could not be established. The reaction can proceed by means of the mechanism proposed by Semmelhack (alcohol being oxidised by uncoordinated TEMPO<sup>+</sup> formed upon oxidation of TEMPO by Cu<sup>II</sup>)<sup>[76e]</sup> or by that of Sheldon (copper-centred oxidative dehydrogenation by TEMPO of the alkoxide ligand RCH<sub>2</sub>O<sup>–</sup> derived from the alcohol, to form an R–C'HO radical and TEMPOH)<sup>[76f]</sup> or related ones discussed on the basis of theoretical studies.<sup>[71,76g]</sup> Electron transfer from the R–C'HO radical to Cu<sup>II</sup> leads to the aldehyde RCHO and Cu<sup>I</sup>. TEMPO-mediated aerobic oxidation of Cu<sup>I</sup> regenerates Cu<sup>II</sup>, whereas TEMPO is regenerated upon aerobic oxidation of TEMPOH.<sup>[31,71,76a,76b,76d,76f,76h]</sup> Furthermore, the anti-oxidant ability of TEMPO to suppress the further oxidation of aldehyde to acid is also known, acting as a radical scavenger and terminating free radical chains.<sup>[63,76h]</sup> The interaction of TEMPO with a copper catalyst precursor was confirmed in our systems by the detection of the adduct [CuL<sup>5</sup>(TEMPO)]<sup>+</sup> [*m/z* (%) = 744 (10)] in the ESI-MS(+) spectra of reaction solutions (diluted with MeOH) containing CuL<sup>5</sup>, benzyl alcohol and TEMPO in MeCN/aqueous solution.

The above discussed mechanisms are distinct from that of galactose oxidase, which catalyses the oxidation of D-galactose to D-galactohexodialdose where a protein-bound phenoxyl radical, coordinated to Cu, behaves as an H-atom abstractor from the alkoxide ligand.<sup>[76b]</sup> In our copper system, such a role is played by TEMPO and not by the Schiff base ligand.

## Conclusion

Copper(II) complexes CuL<sup>1–5</sup> with five new Schiff bases based on 2-hydroxybenzaldehyde, 2,4-dihydroxybenzaldehyde, 3,5-dibromo-2-hydroxybenzaldehyde, 2-hydroxy-5-nitrobenzaldehyde, 2-chloro-2-hydroxybenzaldehyde and 1,3-bis(3-aminopropyl)tetramethyldisiloxane, respectively, which contain a tetramethyldisiloxane unit, have been prepared *in situ* and characterised by FTIR, UV/Vis, EPR spectroscopy and X-ray diffraction methods. Charge density calculations performed on CuL<sup>1</sup> along with DFT calculations provided evidence for high ionicity of the Si–O bonds in the tetramethyldisiloxane unit. The formation of a 12-membered central chelate ring in these complexes is presumably governed by the tetramethyldisiloxane unit, which separates the aliphatic chains, thus significantly reducing the mechanical strain in a 12-membered chelate ring. We can call this a chemical analogy to a shoulder yoke, which spreads out the load on the bearer. Copper(II)–salen-type Schiff base complexes bearing a disiloxane moiety, in particular those with electron-withdrawing substituents (chloro, bromo, and nitro) in the aromatic ring, show high catalytic activity and selectivity in the aerobic oxidation of benzyl alcohol to benzaldehyde mediated by the TEMPO radical, under mild conditions (aqueous acetonitrile at 50 °C – a solvent system environmentally more friendly than neat organic solvents). The presence of a base

is fundamental and potassium carbonate, with a low coordinating ability, is the best one among those screened.

## Experimental Section

**Starting Materials:** 1,3-Bis(3-aminopropyl)tetramethyldisiloxane,  $[\text{H}_2\text{N}(\text{CH}_2)_3(\text{CH}_3)_2\text{Si}]_2\text{O}$ , benzyl alcohol, and 2,2,6,6-tetramethylpiperidine-1-oxyl (TEMPO) were purchased from Fluka and Aldrich. Copper(II) chloride dihydrate, copper(II) acetate monohydrate and copper(II) nitrate, 2-hydroxybenzaldehyde, 2,4-dihydroxybenzaldehyde, 3,5-dibromo-2-hydroxybenzaldehyde, 2-hydroxy-5-nitrobenzaldehyde and 5-chloro-2-hydroxybenzaldehyde were from Aldrich, pyridine from Fluka and 4-methylpyridine (4-Me-Py) from Merck.

**Physical Measurements:** Fourier transform infrared (FTIR) spectra were recorded by using a Bruker Vertex 70 FTIR spectrometer. Analyses were performed in the transmission mode in the range 400–4000  $\text{cm}^{-1}$  at room temperature with a resolution of 2  $\text{cm}^{-1}$  and accumulation of 32 scans. The samples were incorporated in dry KBr and measured as pellets.  $^1\text{H}$  NMR spectra were acquired in  $\text{CDCl}_3$  at 25 °C with a Bruker Avance DRX 400 MHz spectrometer operating at 400.13 MHz. Chemical shifts are reported in ppm and are referenced to chloroform [ $\delta(^1\text{H}) = 7.26$  ppm]. EPR spectra were recorded at 77 K with a modified Varian E-4 spectrometer as described previously.<sup>[77]</sup> Electrospray ionisation mass spectrometry (ESI-MS) was carried out with a Bruker Esquire 3000 instrument, and the samples were dissolved in methanol.

**X-ray Diffraction Measurements:** Crystallographic measurements were carried out with an Oxford-Diffraction XCALIBUR E CCD diffractometer by using graphite-monochromated Mo- $K_\alpha$  radiation. The crystals were placed at 40 mm from the detector. The unit cell determination and data integration were carried out by using the CrysAlis package of Oxford Diffraction.<sup>[78]</sup> All structures were solved by direct methods using SHELXS-97 and refined by full-

matrix least squares on  $F_o^2$  with SHELXL-97<sup>[79]</sup> with anisotropic displacement parameters for non-hydrogen atoms. All H atoms attached to carbon atoms were introduced in idealised positions ( $d_{\text{CH}} = 0.96$  Å) by using the riding model with  $U_{\text{iso}}(\text{H}) = 1.2U_{\text{eq}}(\text{parent C atom})$ . Positional parameters of the H atoms for the  $\text{H}_2\text{O}$  molecule and OH groups were verified by the geometric parameters of the corresponding hydrogen bonds. The main crystallographic data together with refinement details are summarised in Tables 8 and 9. Selected bond lengths and bond angles are given in Table 1, while those for  $[\text{CuL}^3][\text{Cu}(\text{4-Me-Py})_4\text{Cl}]\text{Cl}$  are in the caption of Figure 3. CCDC-883049 (for  $\text{CuL}^1$ ), -883050 (for  $\text{CuL}^1 \cdot 0.5\text{Py}$ ), -883051 (for  $\text{CuL}^2 \cdot 0.375\text{CH}_2\text{Cl}_2$ ), -883052 (for  $[\text{CuL}^3][\text{Cu}(\text{4-Me-Py})_4\text{Cl}]\text{Cl} \cdot 2\text{H}_2\text{O}$ ), -883053 (for  $\text{CuL}^4$ ), -883054 (for  $\text{CuL}^4 \cdot \text{CHCl}_3$ ), -883055 (for  $\text{CuL}^5$ ) contain the supplementary crystallographic data for this paper. These data can be obtained free of charge from The Cambridge Crystallographic Data Centre via [www.ccdc.cam.ac.uk/data\\_request/cif](http://www.ccdc.cam.ac.uk/data_request/cif).

**DFT Calculations:** The geometry of  $\text{CuL}^1$  in the doublet spin state was optimised (by starting from the experimental X-ray diffraction structure) at the B3LYP level of theory by using standard 6-311G\* basis sets of the Gaussian 03 library for all atoms without any symmetry restrictions with the Gaussian 03 program package.<sup>[80]</sup> The stability of the obtained structures was tested by vibrational analysis (no imaginary vibrations). The electronic structure of  $\text{CuL}^1$  was investigated by using QTAIM (Quantum Theory of Atoms-in-Molecule) topological analysis of electron density.<sup>[62]</sup> The results are evaluated in terms of atomic charges  $q$  obtained by the electron-density integration over atomic basins (up to the 0.001  $\text{eBohr}^{-3}$  level). Bond characteristics were evaluated in terms of electron density  $\rho$ , its Laplacian  $\nabla^2\rho$  [Equation (2)]:

$$\nabla^2\rho = \lambda_1 + \lambda_2 + \lambda_3 \quad (2)$$

and bond ellipticity  $\varepsilon$  [Equation (3)]:

$$\varepsilon = \lambda_1/\lambda_2 - 1 \quad (3)$$

Table 8. Crystallographic data, details of data collection and structure refinement parameters for  $\text{CuL}^1$ ,  $\text{CuL}^1 \cdot 0.5\text{Py}$ ,  $\text{CuL}^2 \cdot 0.375\text{CH}_2\text{Cl}_2$ ,  $[\text{CuL}^3][\text{Cu}(\text{4-Me-Py})_4\text{Cl}]\text{Cl} \cdot 2\text{H}_2\text{O}$ .

	$\text{CuL}^1$	$\text{CuL}^1 \cdot 0.5\text{Py}$	$\text{CuL}^2 \cdot 0.375\text{CH}_2\text{Cl}_2$	$[\text{CuL}^3][\text{Cu}(\text{4-Me-Py})_4\text{Cl}]\text{Cl} \cdot 2\text{H}_2\text{O}$
Empirical formula	$\text{C}_{24}\text{H}_{34}\text{CuN}_2\text{O}_3\text{Si}_2$	$\text{C}_{53}\text{H}_{73}\text{Cu}_2\text{N}_5\text{O}_6\text{Si}_4$	$\text{C}_{195}\text{H}_{246}\text{Br}_{32}\text{Cl}_6\text{Cu}_8\text{N}_{16}\text{O}_{24}\text{Si}_{16}$	$\text{C}_{48}\text{H}_{66}\text{Cl}_2\text{Cu}_2\text{N}_6\text{O}_7\text{Si}_2$
$M_r$	518.25	1115.60	6925.66	1093.23
$T$ [K]	200(2)	293(2)	293(2)	293(2)
$\lambda$ [Å]	0.71073	0.71073	0.71073	0.71073
Crystal system	monoclinic	triclinic	monoclinic	monoclinic
Space group	$C2/c$	$P\bar{1}$	$P2_1/c$	$C2/c$
$a$ [Å]	21.6361(16)	12.3215(15)	20.838(3)	18.558(2)
$b$ [Å]	11.067(3)	15.3519(17)	12.7452(8)	9.9019(10)
$c$ [Å]	23.2134(13)	18.583(3)	26.593(5)	29.742(4)
$\alpha$ [°]	90	68.055(12)	90	90
$\beta$ [°]	105.529(8)	75.606(12)	109.519(18)	102.925(13)
$\gamma$ [°]	90	67.293(11)	90	90
$V$ [Å <sup>3</sup> ]	5355.5(15)	2985.3(7)	6656.9(16)	5326.8(11)
$Z$	8	2	1	4
$\rho_{\text{calcd}}$ [ $\text{g cm}^{-3}$ ]	1.286	1.241	1.729	1.363
Crystal size [mm]	$0.60 \times 0.40 \times 0.40$	$0.25 \times 0.20 \times 0.15$	$0.40 \times 0.05 \times 0.02$	$0.10 \times 0.05 \times 0.01$
Reflections collected/unique	11938/5248 ( $R_{\text{int}} = 0.0229$ )	17339/11568 ( $R_{\text{int}} = 0.0736$ )	35767/13063 ( $R_{\text{int}} = 0.0886$ )	9342/5174 ( $R_{\text{int}} = 0.0884$ )
$\mu$ [ $\text{mm}^{-1}$ ]	0.931	0.841	5.618	0.997
$R_1$ [a] [ $I > 2\sigma(I)$ ]	0.0333	0.0689	0.0828	0.0846
$R_1$ [b] (all data)	0.0442	0.1247	0.1865	0.2353
GOF [c]	1.051	0.999	1.013	0.956
$\Delta\rho_{\text{max/min}}$ [ $\text{e Å}^{-3}$ ]	0.357/−0.336	0.583/−0.452	1.383/−1.372	0.630/−0.537

[a]  $R_1 = \sum |F_o| - |F_c| / \sum |F_o|$ . [b]  $wR_2 = \{\sum [w(F_o^2 - F_c^2)^2] / \sum [w(F_o^2)^2]\}^{1/2}$ . [c]  $\text{GOF} = \{\sum [w(F_o^2 - F_c^2)^2] / (n - p)\}^{1/2}$ ;  $n$  = number of reflections,  $p$  = total number of parameters refined.

Table 9. Crystallographic data, details of data collection and structure refinement parameters for CuL<sup>4</sup>, CuL<sup>4</sup>·CHCl<sub>3</sub> and CuL<sup>5</sup>.

	CuL <sup>4</sup>	CuL <sup>4</sup> ·CHCl <sub>3</sub>	CuL <sup>5</sup>
Empirical formula	C <sub>24</sub> H <sub>32</sub> CuN <sub>4</sub> O <sub>7</sub> Si <sub>2</sub>	C <sub>25</sub> H <sub>33</sub> Cl <sub>3</sub> CuN <sub>4</sub> O <sub>7</sub> Si <sub>2</sub>	C <sub>24</sub> H <sub>32</sub> Cl <sub>2</sub> CuN <sub>2</sub> O <sub>3</sub> Si <sub>2</sub>
<i>M<sub>r</sub></i>	608.26	727.62	587.14
<i>T</i> [K]	293(2)	293(2)	293(2)
<i>λ</i> [Å]	0.71073	0.71073	0.71073
Crystal system	monoclinic	triclinic	monoclinic
Space group	<i>C</i> 2/ <i>c</i>	<i>P</i> $\bar{1}$	<i>P</i> 2 <sub>1</sub> / <i>c</i>
<i>a</i> [Å]	35.797(9)	9.5865(3)	15.1286(8)
<i>b</i> [Å]	9.3728(7)	13.0494(5)	12.1703(8)
<i>c</i> [Å]	25.292(6)	13.2635(5)	31.983(2)
<i>α</i> [°]	90	96.237(3)	90
<i>β</i> [°]	134.27(4)	93.386(3)	103.450(6)
<i>γ</i> [°]	90	96.310(3)	90
<i>V</i> [Å <sup>3</sup> ]	6077(2)	1635.18(10)	5727.2(6)
<i>Z</i>	8	2	8
<i>ρ</i> <sub>calcd.</sub> [g cm <sup>-3</sup> ]	1.330	1.478	1.362
Crystal size [mm]	0.25 × 0.15 × 0.15	0.25 × 0.15 × 0.10	0.20 × 0.10 × 0.10
Reflections collected/unique	21968/5963 ( <i>R</i> <sub>int</sub> = 0.0907)	22821/6400 ( <i>R</i> <sub>int</sub> = 0.0239)	29637/11225 ( <i>R</i> <sub>int</sub> = 0.0550)
<i>μ</i> [mm <sup>-1</sup> ]	0.843	1.033	1.060
<i>R</i> <sub>1</sub> <sup>[a]</sup> [ <i>I</i> > 2σ( <i>I</i> )]	0.0756	0.0663	0.0701
<i>R</i> <sub>1</sub> <sup>[b]</sup> (all data)	0.1856	0.0726	0.1299
GOF <sup>[c]</sup>	1.020	1.011	1.016
Δ <i>ρ</i> <sub>max/min</sub> [e Å <sup>-3</sup> ]	0.423/−0.249	1.513/−1.659	0.756/−0.816

[a]  $R_1 = \sum ||F_o| - |F_c|| / \sum |F_o|$ . [b]  $wR_2 = \{ \sum [w(F_o^2 - F_c^2)^2] / \sum [w(F_o^2)^2] \}^{1/2}$ . [c]  $GOF = \{ \sum [w(F_o^2 - F_c^2)^2] / (n - p) \}^{1/2}$ ; *n* = number of reflections, *p* = total number of parameters refined.

at bond critical points (BCP) where  $\lambda_1 < \lambda_2 < 0 < \lambda_3$  are the eigenvalues of the Hessian of the BCP electron density. PROAIMV software<sup>[81,82]</sup> was used for QTAIM analysis of Gaussian 03 results. Alternatively, NBO (Natural Bond Orbital) analysis<sup>[83]</sup> (in terms of atomic charges and bond occupancies) was performed. MOLEKEL software<sup>[84]</sup> was used for visualisation purposes.

**Data Collection for Experimental Charge-Density Analysis:** A single crystal of CuL<sup>1</sup> was selected and mounted in the cold nitrogen stream. The data were collected at 100.0(1) K with an Oxford Diffraction Kappa geometry GEMINI R diffractometer equipped with a Rubi CCD area detector by using graphite-monochromated Mo-*K*<sub>α</sub> radiation ( $\lambda = 0.71073$  Å) at 50 kV and 40 mA. Crystal-to-detector distance was 53 mm. The diffraction data were collected with a large and equally distributed redundancy at eight different detector positions:  $2\theta = \pm 10.97, \pm 24.90, \pm 38.91$  and  $\pm 66.22^\circ$ , where  $\theta$  is the Bragg angle. The strategy was to measure with 53  $\omega$  runs with a frame width of 1.0°. According to the  $\theta$  dependence of the diffracted intensities, the chosen exposure times were 24, 48, 90 and 120 s, respectively. The maximum resolution reached at this experimental setting was 1.13 Å<sup>-1</sup>. A total of 472405 symmetry-equivalent and redundant intensities were collected and integrated, and the Lorentz-polarisation and a FACE-absorption correction were performed with CrysAlis CCD RED software.<sup>[78]</sup> Average redundancy was 14.3 with an internal agreement of 2.60% and  $R(\sigma) = 0.012$ . A total of 448105 reflections were used for multipole refinement. Details of the X-ray diffraction experiment conditions and the crystallographic data for CuL<sup>1</sup> are given in Table S4. The crystal structure was solved and refined by using SHELXS-97 and SHELXL-97.<sup>[79]</sup> Starting parameters for multipole refinement were taken from a routine SHELXL refinement, and all other refinements were carried out on *F*<sup>2</sup> by using the XD suite of programs.<sup>[85]</sup> As the equivalent data are collected with a different value of TBAR (distance of primary and diffracted beam through the crystal), all nonaveraged data were used in the refinements. A complete atom-centred multipole refinement was carried out with the nonspherical atomic electron density given by the expression:<sup>[86]</sup>

$$\rho_{\text{at}}(r) = P_c \rho_{\text{core}}(r) + P_v \kappa^3 \rho_{\text{valence}}(\kappa r) + \sum_{l=1}^{\text{max}} \kappa'^3 R_l(\kappa' r) \sum_{m=0}^l P_{lm\pm} d_{lm\pm}(\theta, \phi).$$

The H atoms were treated with one bond-directed dipole (*l* = 1), other atoms were refined up to octapoles, for Cu and Si atoms the hexadecapole level (*l*<sub>max</sub> = 4) was used. The local coordinate systems to define multipoles were used as follows: for non-hydrogen atoms: *x*-axis – direction to the closest atom, *y*-axis – perpendicular to the *x*-axis and oriented towards the second closest atom; for hydrogen atoms: *z*-axis – direction to the bonding carbon atom and *x*-axis – perpendicular to the *z*-axis. The same type of hydrogen atoms (sp<sup>3</sup> or sp<sup>2</sup> hybridisation) was constrained to have the identical multipole expansions. The strategy for refinement was as described previously.<sup>[87]</sup> The results of refinement are summarised in Table 2.

### Synthesis of Complexes

**CuL<sup>1</sup>:** A solution of 1,3-bis(3-aminopropyl)tetramethyldisiloxane (1.02 g, 4.1 mmol) in methanol (5 mL) was added, whilst stirring at room temperature, to a solution of 2-hydroxybenzaldehyde (1.00 g, 8.2 mmol) in methanol (5 mL). The mixture was stirred at 60 °C for 3 h. The orange solution was then added to a solution of CuCl<sub>2</sub>·2H<sub>2</sub>O (0.70 g, 4.1 mmol) in methanol/dichloromethane (2:1) (6 mL). The mixture was stirred at room temperature for 10 min. A clear dark-green solution generated prismatic dark-green crystals of good quality upon standing at room temperature after 3–4 h. These were separated by filtration, washed with methanol and dried in air. Yield 0.68 g (32.0%). C<sub>24</sub>H<sub>34</sub>CuN<sub>2</sub>O<sub>3</sub>Si<sub>2</sub> (518.26): calcd. C 55.62, H 6.61, N 5.41; found C 55.49, H 6.39, N 5.35. IR (KBr pellet, selected bands):  $\tilde{\nu}_{\text{max}} = 3051, 3025$  (m, C–H aromatic), 2951, 2921 (m, C–H from Si–CH<sub>3</sub>), 2907 (m, C–H aliphatic), 1625 (s, C=N), 1600, 1538 (aromatic ring), 1448 (m, CH<sub>2</sub>), 1394 (m, br.), 1251 (s, Si–CH<sub>3</sub>), 1081 (s, Si–O–Si), 799 (s, Si–CH<sub>3</sub>), 577, 609, 469 cm<sup>-1</sup>. UV/Vis (CHCl<sub>3</sub>):  $\lambda$  ( $\epsilon$ ) = 367 (10315), 306 (9340), 268 (19990 M<sup>-1</sup> cm<sup>-1</sup>) nm. ESI-MS, positive (CH<sub>3</sub>OH): *m/z* = 518 [M + H]<sup>+</sup>, 540 [M + Na]<sup>+</sup>, 1057 [2M + Na]<sup>+</sup>. By starting from copper(II)

acetate or copper(II) nitrate the same product was obtained in a yield of 32.3 and 14.9%, respectively. The identity of the products was established by comparing their IR spectra with that of  $\text{CuL}^1$  prepared from copper(II) chloride, the structure of which has been confirmed by X-ray diffraction (vide infra).

**$\text{CuL}^1 \cdot 0.5\text{Py}$ :** To  $\text{CuL}^1$  (0.21 g, 0.40 mmol) in a mixture of dichloromethane (5 mL) and toluene (2 mL) was added pyridine (0.4 g, 0.5 mmol), and the resultant green solution was stirred at room temperature for 10 min, filtered and allowed to stand undisturbed at room temperature. Dark-green prismatic crystals formed were separated after 3–4 d by filtration, washed with methanol and dried in air. Yield 0.19 g (85.1%).  $\text{C}_{26.5}\text{H}_{36.5}\text{CuN}_{2.5}\text{O}_3\text{Si}_2$  (557.81): calcd. C 57.06, H 6.60, N 6.28; found C 56.85, H 6.83, N 5.85. IR (KBr pellet, selected bands):  $\tilde{\nu}_{\text{max}} = 3050, 3023$  (m, C–H aromatic), 2954, 2926 (m, C–H from Si–CH<sub>3</sub>), 2909 (m, C–H aliphatic), 1626 (s, C=N), 1600, 1538 (aromatic ring), 1449 (m, CH<sub>2</sub>), 1394 (m br.), 1251 (s, Si–CH<sub>3</sub>), 1074 (s, Si–O–Si), 799 (s, Si–CH<sub>3</sub>), 608, 471, 451  $\text{cm}^{-1}$ . ESI-MS, positive ( $\text{CH}_3\text{OH}$ ):  $m/z = 518$  [M + H]<sup>+</sup>, 540 [M + Na]<sup>+</sup>, 1057 [2M + Na]<sup>+</sup>.

**$\text{CuL}^2$ :** 1,3-Bis(3-aminopropyl)tetramethyldisiloxane (0.22 g, 0.9 mmol) in  $\text{CH}_3\text{OH}/\text{CH}_2\text{Cl}_2$  (1:1) (5 mL) was added to a solution of 3,5-dibromosalicylaldehyde (0.51 g, 1.8 mmol) in  $\text{CH}_3\text{OH}/\text{CH}_2\text{Cl}_2$  (1:1) (5 mL) whilst stirring. The reaction mixture was heated at 60 °C for 3 h and then slowly poured into a solution of  $\text{Cu}(\text{OAc})_2 \cdot \text{H}_2\text{O}$  (0.20 g, 1.0 mmol) in  $\text{CH}_2\text{Cl}_2/\text{THF}$  (3:1) (8 mL). The mixture was stirred at room temperature for 10 min and then allowed to stand undisturbed. Dark-green small crystals formed were separated after 3 d, washed with methanol and dried in air. Yield 0.26 g (34.0%).  $\text{C}_{24.375}\text{H}_{29.75}\text{Br}_{1.75}\text{Cl}_{0.75}\text{CuN}_2\text{O}_2\text{Si}_2$  (848.68): calcd. C 34.50, H 3.53, N 3.30; found C 34.35, H 3.46, N 3.17. IR (KBr pellet, selected bands):  $\tilde{\nu}_{\text{max}} = 3066$  (m, C–H aromatic), 2953, 2924 (m, C–H from Si–CH<sub>3</sub>), 1624 (s, C=N), 1581, 1509 (aromatic ring), 1443 (m, CH<sub>2</sub>), 1253 (s, Si–CH<sub>3</sub>), 1065 (s, Si–O–Si), 783 (s, Si–CH<sub>3</sub>), 619, 475, 414  $\text{cm}^{-1}$ . UV/Vis ( $\text{CHCl}_3$ ):  $\lambda(\epsilon) = 394$  sh (9470), 379 (10610), 304 (11536), 279 (21866  $\text{M}^{-1}\text{cm}^{-1}$ ) nm. ESI-MS, positive ( $\text{CH}_3\text{OH}$ ):  $m/z = 856$  [M + Na]<sup>+</sup>.

**$\text{H}_2\text{L}^3$ :** 1,3-Bis(3-aminopropyl)tetramethyldisiloxane (0.90 g, 3.6 mmol) in methanol (5 mL) was slowly added whilst stirring to a solution of 2,4-dihydroxybenzaldehyde (1.00 g, 7.2 mmol) in methanol (20 mL). The reaction mixture was heated to reflux for 10 h, allowed to cool to room temperature and filtered. The filtrate was poured into excess water, and the yellow precipitate formed was filtered off, washed with methanol and dried in air. Yield 1.35 g (76.7%).  $\text{C}_{24}\text{H}_{36}\text{N}_2\text{O}_5\text{Si}_2$  (488.72): calcd. C 58.98, H 7.42, N 5.73; found C 58.49, H 6.57, N 5.84. IR (KBr pellet, selected bands):  $\tilde{\nu}_{\text{max}} = 3053$  (m, C–H aromatic), 2953, 2928 (m, C–H from Si–CH<sub>3</sub>), 2900 (m), 2876 (m), 1642 (s, C=N), 1538 (aromatic ring), 1474 (m, CH<sub>2</sub>), 1253 (s, Si–CH<sub>3</sub>), 1080 (s, Si–O–Si), 793 (s, Si–CH<sub>3</sub>)  $\text{cm}^{-1}$ . <sup>1</sup>H NMR (400.13 MHz,  $\text{CDCl}_3$ ):  $\delta = 8.30$  (s, 1 H, CH=N), 7.14 (s, 1 H, Ar), 6.22 (s, 1 H, Ar), 6.13 (s, 1 H, Ar), 3.47 (s, 2 H, N–CH<sub>2</sub>–), 1.60 (s, 2 H, –CH<sub>2</sub>–CH<sub>2</sub>–CH<sub>2</sub>–), 0.53 (s, 2 H, –CH<sub>2</sub>–Si–), 0.06 [s, 6 H, (CH<sub>3</sub>)<sub>2</sub>Si–O–] ppm.

**[CuL<sup>3</sup>][Cu(4-Me-Py)<sub>4</sub>Cl][Cl·2H<sub>2</sub>O]:** A solution of  $\text{CuCl}_2 \cdot 2\text{H}_2\text{O}$  (0.38 g, 2.24 mmol) in methanol (5 mL) was slowly added to a solution of  $\text{H}_2\text{L}^3$  (0.55 g, 1.12 mmol) in methanol (10 mL) at room temperature. The mixture was stirred for 10 min, and then toluene (10 mL) and 4-methylpyridine (0.2 mL) were added. The solution was allowed to stand undisturbed at room temperature. Green prismatic crystals were filtered off after 3–4 d, washed with methanol and dried in air. Yield 0.4 g (32.7%).  $\text{C}_{48}\text{H}_{66}\text{Cl}_2\text{Cu}_2\text{N}_6\text{O}_7\text{Si}_2$  (1093.24): calcd. C 52.73, H 6.09, N 7.69; found C 53.22, H 5.88, N 7.62. IR (KBr pellet, selected bands):  $\tilde{\nu}_{\text{max}} = 3050, 3023$  (m, C–

H aromatic), 2949, 2918 (m, C–H from Si–CH<sub>3</sub>), 2905 (m, C–H aliphatic), 2856 (m), 1622 (s, C=N), 1537 (aromatic ring), 1446 (m, CH<sub>2</sub>), 1253 (s, Si–CH<sub>3</sub>), 1071 (s, Si–O–Si), 799 (s, Si–CH<sub>3</sub>), 603, 476, 462  $\text{cm}^{-1}$ . UV/Vis ( $\text{CHCl}_3$ ):  $\lambda(\epsilon) = 353$  (14970), 306 sh (18556), 289 (36892), 256 (47516  $\text{M}^{-1}\text{cm}^{-1}$ ) nm. ESI-MS, positive ( $\text{CH}_3\text{OH}$ ):  $m/z = 572$  [M + Na]<sup>+</sup>, 1121 [2M + Na]<sup>+</sup>.

**$\text{CuL}^4$ :** A solution of 2-hydroxy-5-nitrobenzaldehyde (0.61 g, 3.62 mmol) in  $\text{CH}_3\text{OH}/\text{CH}_2\text{Cl}_2$  (1:1) (10 mL) was added to a solution of 1,3-bis(3-aminopropyl)tetramethyldisiloxane (0.45 g, 1.81 mmol) in  $\text{CH}_3\text{OH}/\text{CH}_2\text{Cl}_2$  (1:1) (10 mL). The mixture was heated at 70 °C (oil bath) for 2 h.  $\text{CuCl}_2 \cdot 2\text{H}_2\text{O}$  (0.31 g, 1.81 mmol) in  $\text{CH}_3\text{OH}/\text{CH}_2\text{Cl}_2$  (1:1) (8 mL) was then added, and the solution was allowed to stand at room temperature. Small crystals of good quality formed very rapidly and were separated by filtration, washed with methanol and dried in air. Yield 0.4 g (36.3%).  $\text{C}_{24}\text{H}_{32}\text{CuN}_4\text{O}_7\text{Si}_2$  (608.26): calcd. C 47.39, H 5.30, N 9.21; found C 46.89, H 4.91, N 9.02. IR (KBr pellet, selected bands):  $\tilde{\nu}_{\text{max}} = 2955$  (w), 2924 (m, C–H from Si–CH<sub>3</sub>), 1632 (s, C=N), 1603 (s), 1555 (m, aromatic ring), 1474 (m, CH<sub>2</sub>), 1317 (vs), 1252 (m, Si–CH<sub>3</sub>), 1059 (m, Si–O–Si), 800 (m), 783 (w, Si–CH<sub>3</sub>), 619, 474 (w), 415 (w)  $\text{cm}^{-1}$ . UV/Vis ( $\text{CHCl}_3$ ):  $\lambda(\epsilon) = 363$  (37200), 450 sh (940  $\text{M}^{-1}\text{cm}^{-1}$ ) nm. ESI-MS, positive ( $\text{CH}_3\text{OH}$ ):  $m/z = 608$  [M + H]<sup>+</sup>, 630 [M + Na]<sup>+</sup>.

**$\text{CuL}^4 \cdot \text{CHCl}_3$ :** A solution of 2-hydroxy-5-nitrobenzaldehyde (1.21 g, 7.21 mmol) in  $\text{CHCl}_3/\text{CH}_3\text{OH}/\text{CH}_2\text{Cl}_2$  (10:7:5) (22 mL) was added to a solution of 1,3-bis(3-aminopropyl)tetramethyldisiloxane (0.90 g, 3.63 mmol) in  $\text{CH}_3\text{OH}/\text{CH}_2\text{Cl}_2$  (3:5) (8 mL). The mixture was heated at 70 °C (oil bath) for 2 h.  $\text{CuCl}_2 \cdot 2\text{H}_2\text{O}$  (0.61 g, 3.6 mmol) in  $\text{CH}_3\text{OH}/\text{CH}_2\text{Cl}_2$  (1:1) (8 mL) was then added, and the solution was allowed to stand at room temperature. Small crystals of good quality formed very rapidly and were separated by filtration, washed with methanol and dried in air. Yield 0.6 g (22.9%).  $\text{C}_{25}\text{H}_{33}\text{Cl}_3\text{CuN}_4\text{O}_7\text{Si}_2$  (727.62): calcd. C 41.27, H 4.57, N 7.70; found C 40.68, H 3.95, N 7.14. IR (KBr pellet, selected bands):  $\tilde{\nu}_{\text{max}} = 2924$  (m, C–H from Si–CH<sub>3</sub>), 1632 (vs), (C=N), 1556 (s, aromatic ring), 1474 (s, CH<sub>2</sub>), 1315 (vs), 1253 (m, Si–CH<sub>3</sub>), 1059 (s, Si–O–Si), 838 (m), 800 (m), 757 (m, Si–CH<sub>3</sub>), 658 (m), 417 (w)  $\text{cm}^{-1}$ . UV/Vis ( $\text{CHCl}_3$ ):  $\lambda(\epsilon) = 450$  (sh, 940), 363 (37200). 363 (37200), 450 (sh, 940  $\text{M}^{-1}\text{cm}^{-1}$ ) nm. ESI-MS, positive ( $\text{CH}_3\text{OH}$ ):  $m/z = 608$  [M + H]<sup>+</sup>, 630 [M + Na]<sup>+</sup>.

**[CuL<sup>5</sup>]:** A solution of 1,3-bis(3-aminopropyl)tetramethyldisiloxane (0.24 g, 0.96 mmol) in  $\text{CH}_3\text{OH}/\text{CHCl}_3$  (2:3) (5 mL) was added whilst stirring at room temperature to a solution of 5-chloro-2-hydroxybenzaldehyde (0.30 g, 1.92 mmol) in  $\text{CH}_3\text{OH}/\text{CHCl}_3$  (1:1) (10 mL), and the mixture was stirred at 60 °C for 3 h. The orange solution was then added to a solution of  $\text{CuCl}_2 \cdot 2\text{H}_2\text{O}$  (0.18 g, 1.04 mmol) in  $\text{CH}_3\text{OH}/\text{CHCl}_3$  (1:1) (4 mL), and the reaction mixture was stirred at room temperature for 10 min. A clear dark-green solution generated prismatic dark-green crystals of good quality after 3–4 h on standing at room temperature. These were separated by filtration, washed with methanol and dried in air. Yield 0.2 g (35.5%).  $\text{C}_{24}\text{H}_{32}\text{Cl}_2\text{CuN}_2\text{O}_3\text{Si}_2$  (587.14): calcd. C 49.09, H 5.49, N 4.77; found C 48.78, H 5.89, N 4.30. IR (KBr pellet, selected bands):  $\tilde{\nu}_{\text{max}} = 3051$  (w, C–H aromatic), 2955 (m), 2926 (s, C–H from Si–CH<sub>3</sub>), 1626 (s, C=N), 1528 (m, aromatic ring), 1462 (s, CH<sub>2</sub>), 1385 (vs), 1254 (s, Si–CH<sub>3</sub>), 1070 (vs., Si–O–Si), 835 (s), 800 (s), 779 (s, Si–CH<sub>3</sub>), 662 (m), 451 (w)  $\text{cm}^{-1}$ . UV/Vis ( $\text{CHCl}_3$ ):  $\lambda(\epsilon) = 452$  sh (735), 378 (5525), 305 (5800). 363 (37200), 450 sh (940  $\text{M}^{-1}\text{cm}^{-1}$ ) nm. ESI-MS, positive ( $\text{CH}_3\text{OH}$ ):  $m/z = 588$  [M + H]<sup>+</sup>.

**Oxidation of a Primary Alcohol (Benzyl Alcohol) by Using TEMPO/Air:** The reactions were carried out in 20 mL round-bot-

tom flasks equipped with condensers under atmospheric pressure of air. Typically, to an MeCN/aqueous solution of  $K_2CO_3$  (1:1) (5.0 mL,  $0.1 \text{ mol L}^{-1}$ ), were added alcohol (3.0 mmol), catalyst ( $3 \mu\text{mol}$ ,  $0.1 \text{ mol}\%$  vs. substrate) and TEMPO (0.15 mmol,  $5 \text{ mol}\%$  vs. substrate). The reaction solutions in all cases were vigorously stirred by using magnetic stirrers, and an oil bath was used to achieve the desired reaction temperature. After the oxidation reaction, the reaction mixtures were neutralised by using  $1 \text{ M HCl}$  and then extracted with ethyl acetate (EtOAc) (10 mL). The organic phase was used for chromatographic analyses by using acetophenone as the internal standard, whereafter a small aliquot was taken and analysed by gas chromatography (GC) using a Fisons Instruments model 8160 gas chromatograph equipped with a DBWAX capillary column (column length 30 m; internal diameter 0.32 mm; film 0.25  $\mu\text{m}$ ; helium as the carrier gas) and an FID detector. GC-MS was also performed by using a Perkin-Elmer model Clarus 600 GC-MS/EI/CI/FID equipped with a BPX5 capillary column (column length 30 m; internal diameter 0.32 mm; film 0.25  $\mu\text{m}$ ; helium as the carrier gas). The ionisation voltage was 70 eV. The products were identified by comparison of their retention times with those of authentic samples and by comparing their mass spectra with fragmentation patterns obtained from the NIST spectral library stored in the computer software of the mass spectrometer.

**Supporting Information** (see footnote on the first page of this article): ORTEP view of  $CuL^1 \cdot 0.5Py$  (molecule A); ORTEP view of  $CuL^4 \cdot CHCl_3$ ; EPR spectra of  $CuL^1 \cdot 0.5Py$ ,  $CuL^2$ ,  $CuL^4$ , and  $CuL^5$ ; ORTEP plot of  $CuL^1$ ; frontier spin orbitals and corresponding orbital energies  $\epsilon$  of  $CuL^1$ ; comparison of experimental bond lengths [ $\text{\AA}$ ] and angles [ $^\circ$ ] with those resulting from DFT calculations of  $CuL^1$ ; NBO bond occupancy and percent of Si contribution for  $CuL^1$ ; effect of base in the aerobic oxidation of benzyl alcohol by the copper(II) salen-type Schiff base complexes  $CuL^{1-5}$  using TEMPO/air.

## Acknowledgments

This research was financially supported by the European Regional Development Fund, Sectoral Operational Programme "Increase of Economic Competitiveness", Priority Axis 2 (SOP IEC-A2-O2.1.2-2009-2, ID 570 COD SMIS-CSNR 12473, contract 129/2010-POLISILMET). The financial support of the Austrian Agency for International Cooperation in Education and Research (OEAD) (contract no. SK01/2011), as well as of the Science and Technology Assistance Agency (contract no. APVV-0202-10) and the Slovak Grant Agency VEGA (contract nos. 1/0679/11, 1/0327/12 and 1/0289/12) is gratefully acknowledged. This work has been partially supported by the Foundation for Science and Technology (FCT), Portugal (projects PTDC/QUI-QUI/102150/2008 and PEst-OE/QUI/UI0100/2011, and grant BPD/46812/2008).

- [1] A. D. Cort, F. Gasparrini, L. Lunazzi, L. Mandolini, A. Mazzanti, C. Pasquini, M. Pierini, R. Rompietti, L. Schiaffino, *J. Org. Chem.* **2005**, *70*, 8877–8883.
- [2] D. A. Atwood, M. J. Harvey, *Chem. Rev.* **2001**, *101*, 37–52.
- [3] Y. Shimazaki, T. Yajima, F. Tani, S. Karasawa, K. Fukui, Y. Naruta, O. Yamauchi, *J. Am. Chem. Soc.* **2007**, *129*, 2559–2568.
- [4] a) D. P. Goldberg, S. J. Lippard, *Adv. Chem. Ser.* **1995**, *246*, 61–81; b) P. Chaudhuri, K. Wieghardt, *Prog. Inorg. Chem.* **2001**, *50*, 151–216; c) B. A. Jazdzewski, W. B. Tolman, *Coord. Chem. Rev.* **2000**, *200–202*, 633–685; d) S. Itoh, M. Taki, S. Fukuzumi, *Coord. Chem. Rev.* **2000**, *198*, 3–20; e) E. Saint-Aman, S. Ménage, J.-L. Pierre, E. Defrancq, G. Gellon, *New J. Chem.* **1998**, *22*, 393–394; f) R. C. Pratt, T. D. P. Stack, *Inorg. Chem.* **2005**, *44*, 2367–2375.
- [5] E. Jungreis, S. Thabet, *Analytical Applications of Schiff Bases*, Marcell Dekker, New York, **1969**.
- [6] I. Sheikhshoaie, M. F. W. Fabian, *Dyes Pigm.* **2006**, *70*, 91–98.
- [7] P. G. Cozzi, *Chem. Soc. Rev.* **2004**, *33*, 410–421.
- [8] a) E. C. Niederhoffer, J. H. Timmons, A. E. Martell, *Chem. Rev.* **1984**, *84*, 137–203; b) C. L. Bailey, R. S. Drago, *Coord. Chem. Rev.* **1987**, *79*, 321–332; c) M. S. Sigman, E. N. Jacobsen, *J. Am. Chem. Soc.* **1998**, *120*, 5315–5316.
- [9] T. P. Yoon, E. N. Jacobsen, *Science* **2003**, *299*, 1691–1693.
- [10] W. Zhang, J. L. Loebach, S. R. Wilson, E. N. Jacobsen, *J. Am. Chem. Soc.* **1990**, *112*, 2801–2803.
- [11] R. Irie, K. Noda, Y. Ito, N. Matsumoto, T. Katsuki, *Tetrahedron Lett.* **1990**, *31*, 7345–7348.
- [12] E. M. McGarrige, D. G. Gilheany, *Chem. Rev.* **2005**, *105*, 1563–1602.
- [13] V. Mirkhani, M. Moghadam, S. Tangestaninejad, I. Mohammadpoor-Baltork, N. Rasouli, *Catal. Commun.* **2008**, *9*, 2411–2416.
- [14] S. Velusamy, T. Punniyamurthy, *Tetrahedron Lett.* **2003**, *44*, 8955–8957.
- [15] M. Salavati-Niasari, M. Bazarganipour, *Appl. Surf. Sci.* **2009**, *255*, 7610–7617.
- [16] S. Velusamy, T. Punniyamurthy, *Eur. J. Org. Chem.* **2003**, 3913–3915.
- [17] Y.-M. Lin, Z. Li, V. Casarotto, J. Ehrmantraut, A. N. Nguen, *Tetrahedron Lett.* **2007**, *48*, 5531–5534.
- [18] W. Sun, E. Herdtweck, F. E. Kühn, *New J. Chem.* **2005**, *29*, 1577–1580.
- [19] K. Dhahagani, J. Rajesh, R. Kannan, G. Rajagopal, *Tetrahedron: Asymmetry* **2011**, *22*, 857–865.
- [20] a) Y. N. Belokon', R. G. Davies, M. North, *Tetrahedron Lett.* **2000**, *41*, 7245–7248; b) Y. N. Belokon', D. Bhave, D. D'Addario, E. Groaz, M. North, V. Tagliazuca, *Tetrahedron* **2004**, *60*, 1849–1861; c) D. Banti, Y. N. Belokon', W.-L. Fu, E. Groaz, M. North, *Chem. Commun.* **2005**, 2707–2709.
- [21] a) H. Milburn, M. R. Truter, B. L. Vickery, *J. Chem. Soc., Dalton Trans.* **1974**, 841–846; b) E. N. Baker, D. Hall, T. N. Waters, *J. Chem. Soc. A* **1970**, 400–405; c) M. M. Bhadbhade, D. Srinivas, *Inorg. Chem.* **1993**, *32*, 6122–6130.
- [22] M. G. B. Drew, R. N. Prasad, R. P. Sharma, *Acta Crystallogr., Sect. C* **1985**, *41*, 1755–1758.
- [23] H.-H. Yao, J.-M. Lo, B.-H. Chen, T.-H. Lu, *Acta Crystallogr., Sect. C* **1997**, *53*, 1012–1013.
- [24] a) B. H. Chen, H. H. Yao, W. T. Huang, P. Chattopadhyay, J. M. Lo, T. H. Lu, *Solid State Sci.* **1999**, *1*, 119–131; b) L. C. Nathan, J. E. Köhne, J. M. Gilmore, K. A. Hannibal, W. E. Dewhirst, T. D. Mai, *Polyhedron* **2003**, *22*, 887–894.
- [25] S. Yamashita, M. Nihei, H. Oshio, *Chem. Lett.* **2003**, *32*, 808–809.
- [26] T. Friscic, A. J. Lough, G. Ferguson, B. Kaitner, *Acta Crystallogr., Sect. C* **2002**, *58*, m313–m315.
- [27] a) M. Marcu, M. Cazacu, C. Racles, *Appl. Organomet. Chem.* **2003**, *17*, 693–700; b) M. Cazacu, M. Marcu, A. Vlad, A. Toth, C. Racles, *J. Polym. Sci., Part A* **2003**, *1*, 3169–3179; c) M. Cazacu, A. Airinei, M. Marcu, *Appl. Organomet. Chem.* **2002**, *16*, 643–648; d) A. Vlad, C. Turta, M. Cazacu, E. Rusu, S. Shova, *Eur. J. Inorg. Chem.* DOI: 10.1002/ejic.201200612.
- [28] W. Ries, T. Albright, J. Silvestre, I. Bernal, *Inorg. Chim. Acta* **1986**, *111*, 119–128.
- [29] W. Noll, in *Chemistry and Technology of Silicones* (Ed.: W. Noll), Academic Press Inc. (London) Ltd, New York, **1968**.
- [30] G. V. Gibbs, A. F. Wallace, D. F. Cox, R. T. Downs, N. L. Ross, K. M. Rosso, *Am. Mineral.* **2009**, *94*, 1085–1102.
- [31] a) P. J. Figiel, M. N. Kopylovich, J. Lasri, M. F. C. Guedes da Silva, J. J. R. Frausto da Silva, A. J. L. Pombeiro, *Chem. Commun.* **2010**, *46*, 2766–2768; b) P. J. Figiel, A. Sibauh, J. U. Ahmad, M. Nieger, M. T. Räisänen, M. Leskelä, T. Repo, *Adv. Synth. Catal.* **2009**, *351*, 2625–2632; c) P. J. Figiel,

- M. Leskelä, T. Repo, *Adv. Synth. Catal.* **2007**, *349*, 1173–1179.
- [32] a) K. T. Mahmudov, M. N. Kopylovich, M. F. C. Guedes da Silva, P. J. Figiel, Y. Y. Karabach, A. J. L. Pombeiro, *J. Mol. Catal. A* **2010**, *318*, 44–50; b) M. N. Kopylovich, K. T. Mahmudov, M. Haukka, P. J. Figiel, A. Mizar, M. F. C. Guedes da Silva, A. J. L. Pombeiro, *Eur. J. Inorg. Chem.* **2011**, 4175–4181; c) A. M. Kirillov, M. N. Kopylovich, M. V. Kirillova, M. Haukka, M. F. G. C. da Silva, A. J. L. Pombeiro, *Angew. Chem.* **2005**, *117*, 4419; *Angew. Chem. Int. Ed.* **2005**, *44*, 4345–4349.
- [33] A. M. Kirillov, M. N. Kopylovich, M. V. Kirillova, E. Y. Karabach, M. Haukka, M. F. G. C. da Silva, A. J. L. Pombeiro, *Adv. Synth. Catal.* **2006**, *348*, 159–174.
- [34] R. R. Fernandes, J. Lasri, M. F. C. Guedes da Silva, J. A. L. da Silva, J. J. R. Frausto da Silva, A. J. L. Pombeiro, *J. Mol. Catal. A* **2011**, *351*, 100–111.
- [35] C. Di Nicola, Y. Y. Karabach, A. M. Kirillov, M. Monari, L. Pandolfo, C. Pettinari, A. J. L. Pombeiro, *Inorg. Chem.* **2007**, *46*, 221–230.
- [36] Y. Y. Karabach, A. M. Kirillov, M. Haukka, M. N. Kopylovich, A. J. L. Pombeiro, *J. Inorg. Biochem.* **2008**, *102*, 1190–1194.
- [37] M. V. Kirillova, A. M. Kirillov, M. F. G. C. da Silva, A. J. L. Pombeiro, *Eur. J. Inorg. Chem.* **2008**, 3423–3427.
- [38] K. R. Gruenwald, A. M. Kirillov, M. Haukka, J. Sanchiz, A. J. L. Pombeiro, *Dalton Trans.* **2009**, 2109–2120.
- [39] L. S. Shul'pina, M. V. Kirillova, A. J. L. Pombeiro, G. B. Shul'pin, *Tetrahedron* **2009**, *65*, 2424–2429.
- [40] S. Contaldi, C. Di Nicola, F. Garau, Y. Y. Karabach, L. M. D. R. S. Martins, M. Monari, L. Pandolfo, C. Pettinari, A. J. L. Pombeiro, *Dalton Trans.* **2009**, 4928–4941.
- [41] C. Di Nicola, F. Garau, Y. Y. Karabach, L. M. D. R. S. Martins, M. Monari, L. Pandolfo, C. Pettinari, A. J. L. Pombeiro, *Eur. J. Inorg. Chem.* **2009**, 666–676.
- [42] D. S. Nesterov, V. N. Kokozay, V. V. Dyakonenko, O. V. Shishkin, J. Jezierska, A. Ozarowski, A. M. Kirillov, M. N. Kopylovich, A. J. L. Pombeiro, *Chem. Commun.* **2006**, 4605–4607.
- [43] T. F. S. Silva, E. C. B. Alegria, L. M. D. R. S. Martins, A. J. L. Pombeiro, *Adv. Synth. Catal.* **2008**, *350*, 706–716.
- [44] G. S. Mishra, J. J. F. da Silva, A. J. L. Pombeiro, *J. Mol. Catal. A* **2007**, *265*, 59–69.
- [45] E. C. B. Alegria, M. V. Kirillova, L. M. D. R. S. Martins, A. J. L. Pombeiro, *Appl. Catal. A* **2007**, *317*, 43–52.
- [46] a) A. M. Kirillov, M. Haukka, M. F. C. G. da Silva, A. J. L. Pombeiro, *Eur. J. Inorg. Chem.* **2005**, 2071–2080; b) G. B. Shul'pin, M. V. Kirillova, T. Sooknoi, A. J. L. Pombeiro, *Catal. Lett.* **2008**, *123*, 135–141.
- [47] G. S. Mishra, E. C. B. A. Alegria, L. M. D. R. S. Martins, J. J. F. da Silva, A. J. L. Pombeiro, *J. Mol. Catal. A* **2008**, *285*, 92–100.
- [48] a) M. N. Kopylovich, A. M. Kirillov, A. K. Baev, A. J. L. Pombeiro, *J. Mol. Catal. A* **2003**, *206*, 163–178; b) R. R. Fernandes, M. V. Kirillova, J. A. L. da Silva, J. J. R. F. Silva, A. J. L. Pombeiro, *Appl. Catal. A* **2009**, *353*, 107–112.
- [49] a) G. Trettenhahn, M. Nagl, N. Neuwirth, V. B. Arion, W. Jary, P. Pöchlauer, W. Schmid, *Angew. Chem.* **2006**, *118*, 2860; *Angew. Chem. Int. Ed.* **2006**, *45*, 2794–2798; b) N. V. Gerbeleu, S. S. Palanciuc, Y. A. Simonov, A. A. Dvorkin, P. N. Bourosh, M. T. Reetz, V. B. Arion, K. Töllner, *Polyhedron* **1995**, *14*, 521–527.
- [50] a) M. Handke, W. Jastrzebski, *J. Mol. Struct.* **2004**, *704*, 63–69; b) H. Liu, S. Kondo, N. Takeda, M. Unno, *J. Am. Chem. Soc.* **2008**, *130*, 10074–10075.
- [51] I. Bar-Nahum, H. Cohen, R. Neumann, *Inorg. Chem.* **2003**, *42*, 3677–3684.
- [52] A. Fereday, D. M. L. Goodgame, P. D. Lickiss, S. J. Rooke, A. J. P. White, D. J. Williams, *Inorg. Chem. Commun.* **2002**, *5*, 805–807.
- [53] L. Yang, D. R. Powell, R. P. Houser, *Dalton Trans.* **2007**, 955–964.
- [54] K. Kihara, *Eur. J. Mineral.* **1990**, *2*, 63–77.
- [55] a) G. Glidewell, D. C. Liles, *J. Chem. Soc., Chem. Commun.* **1977**, 632–633; b) K. Suwinska, G. J. Palenik, R. Gerdil, *Acta Crystallogr., Sect. C* **1986**, *42*, 615–620.
- [56] T. Iwamoto, H. Masuda, S. Ishida, C. Kabuto, M. Kira, *J. Am. Chem. Soc.* **2003**, *125*, 9300–9301.
- [57] N. Kocher, J. Henn, B. Gostevskii, D. Kost, I. Kalikhman, B. Engels, D. Stalke, *J. Am. Chem. Soc.* **2004**, *126*, 5563–5568.
- [58] J. Peisach, W. E. Blumberg, *Arch. Biochem. Biophys.* **1974**, *165*, 691–708.
- [59] J. S. Hyde, W. Froncisz, *Annu. Rev. Biophys. Bioeng.* **1982**, *11*, 391–417.
- [60] J. Telser, *J. Braz. Chem. Soc.* **2006**, *17*, 1501–1515.
- [61] C. B. Hübschle, B. Dittrich, *J. Appl. Crystallogr.* **2011**, *44*, 238–240.
- [62] R. F. W. Bader, *Atoms in Molecules: A Quantum Theory*, Clarendon Press, Oxford, **1990**.
- [63] a) A. Dijkman, I. W. C. E. Arends, R. A. Sheldon, *Chem. Commun.* **1999**, 1591–1592; b) C. Punta, C. Gambarotti, “Ideas in Chemistry and Molecular Sciences: Advances in Synthetic Chemistry”, in *N-Hydroxy Derivatives: Key Organocatalysts for the Selective Free Radical Aerobic Oxidation of Organic Compounds* (Ed.: B. Pignataro), Wiley-VCH, Weinheim, **2010**.
- [64] P. J. Figiel, A. M. Kirillov, Y. Y. Karabach, M. N. Kopylovich, A. J. L. Pombeiro, *J. Mol. Catal. A* **2009**, *305*, 178–182.
- [65] S. Velusamy, A. Srinivasan, T. Punniyamurthy, *Tetrahedron Lett.* **2006**, *47*, 923–926.
- [66] P. J. Figiel, A. M. Kirillov, M. F. C. Guedes da Silva, J. Lasri, A. J. L. Pombeiro, *Dalton Trans.* **2010**, *39*, 9879–9888.
- [67] J. U. Ahmada, P. J. Figiel, M. T. Räisänen, M. Leskelä, T. Repo, *Appl. Catal. A* **2009**, *371*, 17–21.
- [68] M. N. Kopylovich, Y. Y. Karabach, K. T. Mahmudov, M. Haukka, A. M. Kirillov, P. J. Figiel, A. J. L. Pombeiro, *Cryst. Growth Des.* **2011**, *11*, 4247–4252.
- [69] R. R. Fernandes, J. Lasri, A. M. Kirillov, M. F. C. Guedes da Silva, J. A. L. da Silva, J. J. R. Frausto da Silva, A. J. L. Pombeiro, *Eur. J. Inorg. Chem.* **2011**, 3781–3790.
- [70] Z. Hu, F. M. Kerton, *Appl. Catal. A* **2012**, *413–414*, 332–339.
- [71] a) C. Michel, P. Belanzoni, P. Gamez, J. Reedijk, E. J. Baerends, *Inorg. Chem.* **2009**, *48*, 11909–11920; b) P. Belanzoni, C. Michel, E. J. Baerends, *Inorg. Chem.* **2011**, *50*, 11896–11904.
- [72] L. Wang, J. Li, Y. Lv, G. Zhao, S. Gao, *Appl. Organomet. Chem.* **2012**, *26*, 37–43.
- [73] a) N. Jiang, A. J. Ragauskas, *Tetrahedron Lett.* **2005**, *46*, 3323–3326; b) S. Velusamy, A. Srinivasan, T. Punniyamurthy, *Tetrahedron Lett.* **2006**, *47*, 923–926; c) S. S. Stahl, *Angew. Chem.* **2004**, *116*, 3480; *Angew. Chem. Int. Ed.* **2004**, *43*, 3400–3420; d) J. W. Wittaker, *Chem. Rev.* **2003**, *103*, 2347–2364; e) N. Mase, T. Mizumori, Y. Taemoto, *Chem. Commun.* **2011**, *47*, 2086–2088; f) R. A. Sheldon, I. W. C. E. Arends, *Adv. Synth. Catal.* **2004**, *346*, 1051–1071.
- [74] Y. H. Ng, I. Izwan, H. Nur, M. N. M. Muhid, H. Hamdan, *J. Fluorine Chem.* **2007**, *128*, 12.
- [75] H. Han, S. Zhang, H. Hou, Y. Fan, Y. Zhu, *Eur. J. Inorg. Chem.* **2006**, 1594–1600.
- [76] a) P. Gamez, I. W. C. E. Arends, J. Reedijk, R. A. Sheldon, *Chem. Commun.* **2003**, 2414–2415; b) P. Gamez, I. Arends, R. Sheldon, J. Reedijk, *Adv. Synth. Catal.* **2004**, *346*, 805–811; c) J. S. Uber, Y. Vogels, D. van den Helder, I. Mutikainen, U. Turpeinen, W. T. Fu, O. Roubeau, P. Gamez, J. Reedijk, *Eur. J. Inorg. Chem.* **2007**, 4197–4206; d) Z. Lu, T. Ladrak, O. Roubeau, J. van der Toorn, S. J. Teat, C. Massera, P. Gamez, J. Reedijk, *Dalton Trans.* **2009**, 3559–3570; e) M. F. Semmelhack, C. R. Schmid, D. A. Cortes, C. S. Chou, *J. Am. Chem. Soc.* **1984**, *106*, 3374–3376; f) A. Dijkman, I. Arends, R. A. Sheldon, *Org. Biomol. Chem.* **2003**, *1*, 3232–3237; g) L. Cheng, J. Wang, M. Wang, Z. Wu, *Inorg. Chem.* **2010**, *49*, 9392–9399; h) A. Dijkman, A. M. González, A. M. Payeras, I. Arends, R. A. Sheldon, *J. Am. Chem. Soc.* **2001**, *123*, 6826–6833.
- [77] V. B. Arion, P. Rapta, J. Telser, S. S. Shova, M. Breza, K. Lušpai, J. Kožisek, *Inorg. Chem.* **2011**, *50*, 2918–2931.

- [78] a) *Agilent CrysAlis PRO*, Agilent Technologies Ltd, Yarnton, England **2011**; b) M. Benaglia, S. Guizzetti, C. Rigamonti, A. Puglisi, *Tetrahedron* **2005**, *61*, 12100–12106.
- [79] G. M. Sheldrick, *Acta Crystallogr., Sect. A* **2008**, *64*, 112–122.
- [80] M. J. Frisch, G. W. Trucks, H. B. Schlegel, G. E. Scuseria, M. A. Robb, J. R. Cheeseman, J. A. Montgomery Jr., T. Vreven, K. N. Kudin, J. C. Burant, J. M. Millam, S. S. Iyengar, J. Tomasi, V. Barone, B. Mennucci, M. Cossi, G. Scalmani, N. Rega, G. A. Petersson, H. Nakatsuji, M. Hada, M. Ehara, K. Toyota, R. Fukuda, J. Hasegawa, M. Ishida, T. Nakajima, Y. Honda, O. Kitao, H. Nakai, M. Klene, X. Li, J. E. Knox, H. P. Hratchian, J. B. Cross, V. Bakken, C. Adamo, J. Jaramillo, R. Gomperts, R. E. Stratmann, O. Yazyev, A. J. Austin, R. Cammi, C. Pomelli, J. W. Ochterski, P. Y. Ayala, K. Morokuma, G. A. Voth, P. Salvador, J. J. Dannenberg, V. G. Zakrzewski, S. Dapprich, A. D. Daniels, M. C. Strain, O. Farkas, D. K. Malick, A. D. Rabuck, K. Raghavachari, J. B. Foresman, J. V. Ortiz, Q. Cui, A. G. Baboul, S. Clifford, J. Cioslowski, B. B. Stefanov, G. Liu, A. Liashenko, P. Piskorz, I. Komaromi, R. L. Martin, D. J. Fox, T. Keith, M. A. Al-Laham, C. Y. Peng, A. Nanayakkara, M. Challacombe, P. M. W. Gill, B. Johnson, W. Chen, M. W. Wong, C. Gonzalez, J. A. Pople, *Gaussian 03*, Revision D.01, Gaussian, Inc., Wallingford, CT, **2004**.
- [81] R. F. W. Bader, T. A. Keith, F. W. Biegler-Koenig, J. A. Duke, K. E. Laidig, R. Bone, J. R. Cheeseman, *Program PROAIMV*, ver. 94, rev. B, McMaster University, Department of Chemistry, Hamilton, Ontario, Canada, **1994**.
- [82] F. W. Biegler-König, R. F. W. Bader, T. Tang, *J. Comput. Chem.* **1982**, *3*, 317–328.
- [83] J. E. Carpenter, F. Weinhold, *J. Mol. Struct.* **1988**, *169*, 41–62.
- [84] U. Varetto, *MOLEKEL*, ver. 5.4.0.8, Swiss National Supercomputing Centre, Manno, Switzerland, **2009**.
- [85] T. Koritsanszky, S. T. Howard, Z. Su, P. R. Mallinson, T. Richter, N. K. Hansen, *XD, Computer Program Package for Multipole Refinement and Analysis of Electron Densities from Diffraction Data*, Free University of Berlin, Germany, **1997**.
- [86] P. Coppens, *X-ray Charge Densities and Chemical Bonding*, Oxford University Press, **1997**.
- [87] K. Kožišek, N. K. Hansen, H. Fuess, *Acta Crystallogr., Sect. B* **2002**, *58*, 463–470.

Received: September 14, 2012  
Published Online: February 4, 2013